Supplementary Information for

Different dimerization affinity and orientation of fluorescent proteins eGFP and eYFP

Yuna Kinoshita,[a] *Yusuke Nakasone,*[b] *Masahide Terazima,*[b] *and Haruko Hosoi*[a]*

[a]Department of Biomolecular Science, Faculty of Science, Toho University, 2-2-1 Miyama, Funabashi 274-8510, Japan

[b]Department of Chemistry, Graduate School of Science, Kyoto University, Kyoto 606-8502, Japan

Contents

SI-1. Amino acid sequences. 2

SI-2. The typical fluorescence decay signals for the anisotropy measurements. 3

SI-3. The sedimentation equilibrium experiments. 4

SI-4. The effect of reabsorption on anisotropy decay at higher concentrations. 7

SI-5. pH dependence of fluorescence anisotropy curves of eGFP and eYFP. 13

SI-6. Observed and calculated fluorescence anisotropy curves. 14

SI-7. Fluorescence anisotropy decay curves of eGFP A206K and eYFP A206K at high concentrations. 40

SI-8. Superimposition of the crystal structures of eGFP and YFP. 41

SI-9. Effect of 203rd Residue on Dimerization behavior of eYFP. 42

SI-10. References. 43

SI-1. Amino acid sequences.

```
eGFP        1 MVSKGEELFTGVVPILVELDGDVNGHKFSVSGEGEGDATYGKLTLKFICT    50
              ||||||||||||||||||||||||||||||||||||||||||||||||||
eYFP        1 MVSKGEELFTGVVPILVELDGDVNGHKFSVSGEGEGDATYGKLTLKFICT    50

eGFP       51 TGKLPVPWPTLVTTLTYGVQCFSRYPDHMKQHDFFKSAMPEGYVQERTIF   100
              ||||||||||||||..||:|||:||||||||||||||||||||||||||||
eYFP       51 TGKLPVPWPTLVTTFGYGLQCFARYPDHMKQHDFFKSAMPEGYVQERTIF   100

eGFP      101 FKDDGNYKTRAEVKFEGDTLVNRIELKGIDFKEDGNILGHKLEYNYNSHN   150
              ||||||||||||||||||||||||||||||||||||||||||||||||||||
eYFP      101 FKDDGNYKTRAEVKFEGDTLVNRIELKGIDFKEDGNILGHKLEYNYNSHN   150

eGFP      151 VYIMADKQKNGIKVNFKIRHNIEDGSVQLADHYQQNTPIGDGPVLLPDNH   200
              ||||||||||||||||||||||||||||||||||||||||||||||||||||
eYFP      151 VYIMADKQKNGIKVNFKIRHNIEDGSVQLADHYQQNTPIGDGPVLLPDNH   200

eGFP      201 YLSTQSALSKDPNEKRDHMVLLEFVTAAGITLGMDELYK   239
              |||.|||||||||||||||||||||||||||||||||||
eYFP      201 YLSYQSALSKDPNEKRDHMVLLEFVTAAGITLGMDELYK   239
```

Figure S1. Amino acid sequences of eGFP and eYFP. Residues 65–67, forming the chromophore, are highlighted in yellow. Residues differing between eGFP and eYFP are shown in bold.

SI-2. The typical fluorescence decay signals for the anisotropy measurements.

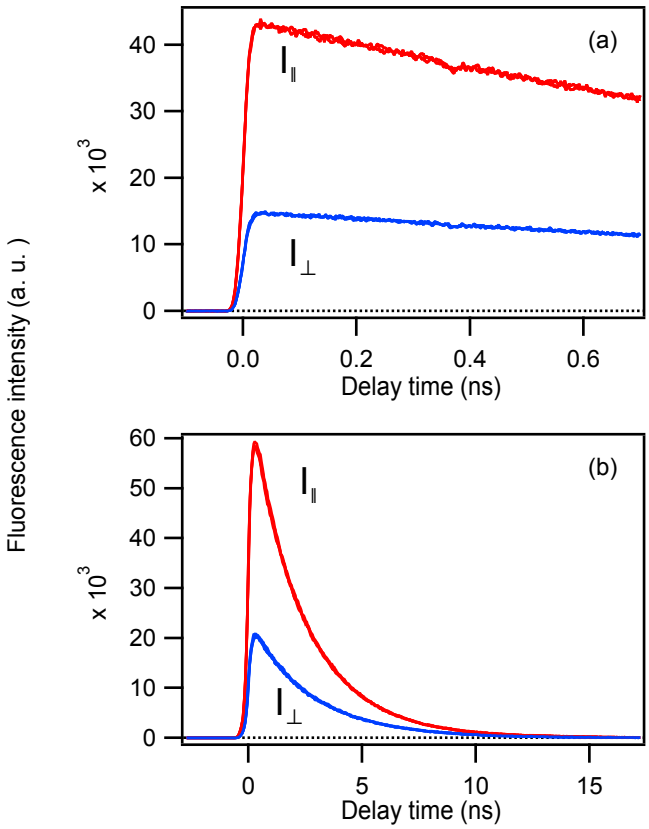

Figure S2. Fluorescence intensities $I_{\parallel}(t)$ (red) and $I_{\perp}(t)$ (blue) of eGFP (1 μM, PBS, pH 7.4) excited at 500 nm. The sweep ranges were (a) 20 ns (4 accumulations) and (b) 1 ns (4 accumulations). Fluorescence signals were spectrally integrated over 520–580 nm.

SI-3. The sedimentation equilibrium experiments.

The equation describing a single ideal species can be expressed as follows:[1, 2]

$$A(r) = A_0 \cdot \exp\left\{\frac{M_{\text{app}}\omega^2}{RT}(1-\bar{v}\rho)\frac{r^2 - r_{\mathbf{r}}^2}{2}\right\} + \text{X} \qquad \text{(S1)}$$

where $A(r)$ and A_0 are the absorbance at radius r and the reference radius $r_{\mathbf{r}}$, respectively; M_{app} is the apparent molecular mass; ω is the angular velocity ($\omega = \text{rpm} \cdot \pi/30$); R is the gas constant; T is the absolute temperature, $(1-\bar{v}\rho)$ is the buoyancy factor; $\bar{v}$ is the partial specific volume; $\rho = 1.000$ g/mL is the density of the buffer; and *X* is a baseline offset. The fitting results are shown in Figure S3 and Table S**1**.

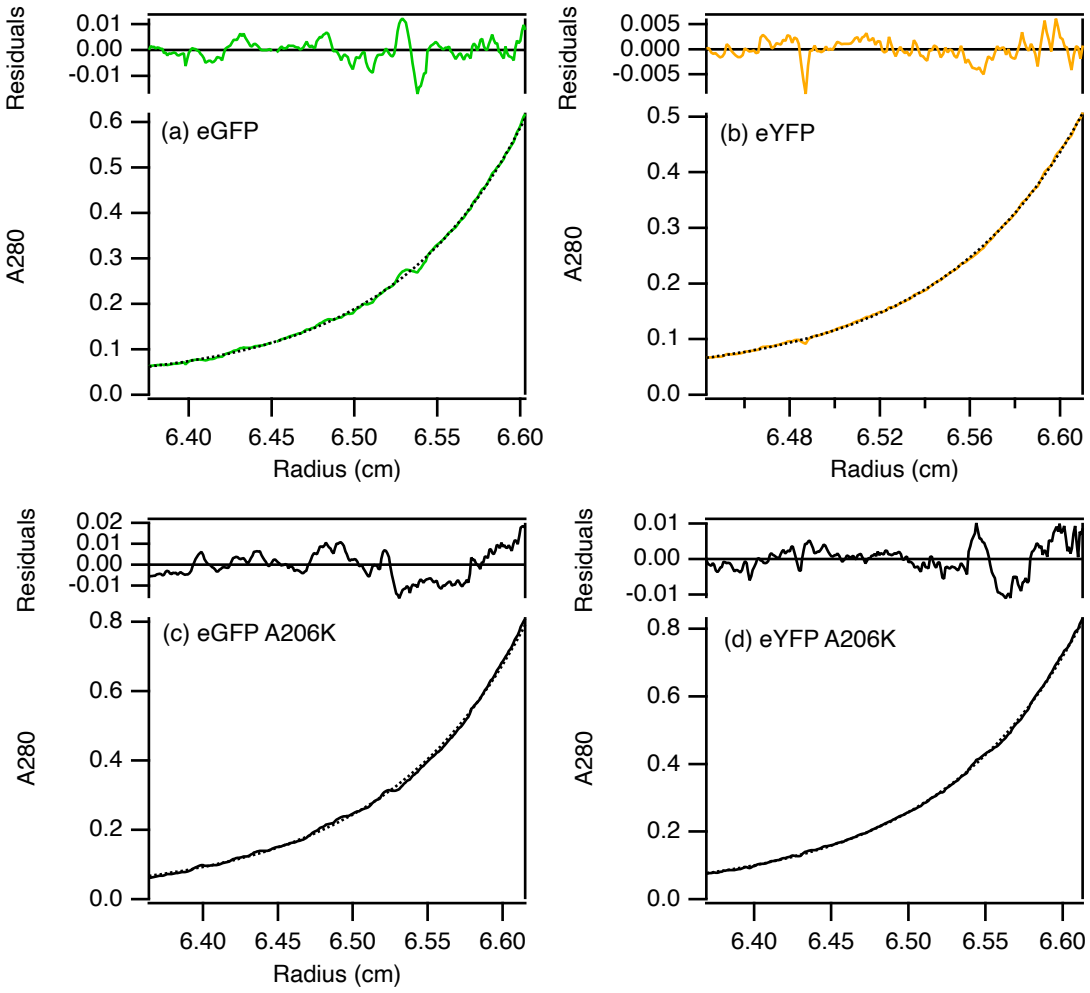

Figure S3. Sedimentation equilibrium analysis of (a) eGFP (17 μM), (b) eYFP (14 μM), (c) eGFP A206K (17 μM), and (d) eYFP A206K (19 μM) (pH 7.4, 20,000 rpm, 25 °C). The solid and dotted lines represent the observed data and calculated curves using eq S1, respectively. The residuals are shown in the upper panels.

Table S1. Parameters for AUC data analysis using the single ideal species model (eq S1). Concentration, rotor speed, reference radius $\boldsymbol{r_r}$, absorbance at $\boldsymbol{r_r}$ ($\boldsymbol{A_0}$), apparent molecular mass ($\boldsymbol{M_{app}}$), and offset X (PBS, pH 7.4, 25 °C)[a]

Sample	Concentration (μM)	Speed (rpm)	r_r (cm)	A_0	M_{app} (g·mol^{-1})	X
eGFP	17	20000	6.376	0.0359 (0.0002)	39600 (100)	0.0265 (0.0005)
eYFP	14	20000	6.443	0.0348 (0.0004)	50100 (200)	0.0319 (0.0006)
eGFP A206K	17	20000	6.364	0.05841 (0.00009)	33330 (20)	0.0091 (0.0002)
eYFP A206K	19	20000	6.369	0.0616 (0.0004)	33990 (70)	0.0157 (0.0005)

[a]Values in parentheses are one standard deviation.

Table S2. Parameters for AUC data analysis of eGFP using the reversible self-association model (eq 6). Concentration, rotor speed, association constant $\boldsymbol{K_A}$, reference radius $\boldsymbol{r_r}$, absorbance at $\boldsymbol{r_r}$ ($\boldsymbol{A_0}$), and offset X (PBS, pH 7.4, 25 °C).[a]

Entry	Concentration (μM)	Speed (rpm)	K_A (M^{-1})	r_r (cm)	A_0	X
a	26	25000	2930 (40)	6.404	0.0501 (0.0002)	0.0023 (0.0009)
b	18	25000	2930 (40)	6.897	0.02862 (0.00008)	0.0203 (0.0007)
c	25	25000	2930 (40)	6.477	0.0999 (0.0003)	-0.029 (0.001)
d	11	25000	2930 (40)	6.924	0.02131 (0.00008)	0.0054 (0.0008)
e	21	25000	2930 (40)	6.408	0.0335 (0.0001)	-0.0089 (0.0007)
F	11	25000	2930 (40)	6.965	0.0367 (0.0001)	0.0004 (0.0009)
g	22	20000	2930 (40)	6.435	0.1413 (0.0005)	-0.009 (0.001)
h	12	20000	2930 (40)	6.869	0.0376 (0.0001)	0.0141 (0.0008)
i	17	20000	2930 (40)	6.376	0.0560 (0.0002)	-0.0095 (0.0009)
j	8	20000	2930 (40)	7.005	0.1043 (0.0007)	0.003 (0.001)

[a]Values in parentheses are one standard deviation.

SI-4. The effect of reabsorption on anisotropy decay at higher concentrations.

Under our experimental conditions, the anisotropy decay signals are free from reabsorption artifacts at concentrations up to 200 μM. Although the decay signals at concentrations of 500 μM and above are affected by reabsorption, the anisotropy value at time 0, $r(0)$, remains unaffected. Detailed discussions are provided below.

At high solute concentrations, fluorescence emitted by excited molecules can be absorbed by other ground-state molecules within the observation volume. This phenomenon, known as reabsorption or radiative energy transfer,[3-5] is distinct from FRET. Fluorescence resulting from reabsorption is depolarized due to the random orientation of molecules in solution. This contribution distorts the observation of other depolarization processes, such as FRET and rotational diffusion, which are the focus of this study. Therefore, it is crucial to eliminate the effect of reabsorption on anisotropy decay.

Fluorescence emitted following reabsorption is temporally delayed relative to the primary emission, resulting in a longer apparent fluorescence lifetime. Here, we consider the case where reabsorption occurs only once, although multiple reabsorption events are possible. The total fluorescence intensity at time t, $I_{\mathrm{tot}}(t)$ is given by[3]

$$I_{\mathrm{tot}}(t) = I_0(1-f)\exp\left(-\frac{t}{\tau}\right) + \frac{I_0 f}{\tau} t \exp\left(-\frac{t}{\tau}\right) \quad \text{(S2)}$$

where I_0 is the initial fluorescence intensity if the excited-state population was produced only by direct excitation, f is the fraction of the excited-state population produced by reabsorption, and τ is the intrinsic fluorescence lifetime. On the right side of the equation, the first term represents the contribution from direct excitation, and the second term represents the reabsorption contribution. The parameter f depends on the optical properties of the molecule, its concentration, and the experimental geometry. Eq S2 indicates the reabsorption contribution is zero at $t = 0$, meaning that the $r(0)$ values are not affected by reabsorption at any concentration.

When the contribution of the second term is small, the observed intensity decay can be approximated by a single exponential function,

$$I_{\mathrm{tot\_app}}(t) = I_{0\_\mathrm{app}}\exp\left(-\frac{t}{\tau_{\mathrm{app}}}\right) \quad \text{(S3)}$$

where $I_{\mathrm{tot\_app}}(t)$ and I_{0_app} are the apparent total fluorescence intensity at time t and

0, respectively, and τ_{app} is the apparent fluorescence lifetime. In the absence of reabsorption, τ_{app} equals τ. In contrast, when reabsorption occurs, τ_{app} becomes larger than τ. Therefore, reabsorption alters the decay kinetics (both intensity and anisotropy), although it does not change the *r*(0) value.

Accordingly, concordance between τ_{app} and τ confirms the absence of reabsorption contributions under specific experimental conditions. To evaluate the reabsorption contribution in this study, the fluorescence decay signals of eGFP A206K under the magic-angle conditions were measured at different concentrations using different path length cells. The results are shown in Figure S4. The apparent fluorescence lifetime τ_{app} for each trace was determined using eq S3 and is displayed in each panel. The decay signals obtained using cells with different path lengths of 0.1 mm, 1 mm, and 10 mm are indistinguishable at 1 μM (Figure S4a), indicating that the determined apparent fluorescence lifetime of 2.5 ns is the intrinsic fluorescence lifetime for eGFP A206K. Similarly, at 10 μM, the decay signals are indistinguishable and the apparent fluorescence lifetimes match the intrinsic value of 2.5 ns (Figure S4b). Therefore, the effect of reabsorption is negligible even when using a 10 mm path length cell. At 100 μM and 200 μM, the decays are slightly slower when using a 1 mm cell compared to a 0.1 mm cell (Figure S4c,d), indicating the onset of reabsorption effects in the thicker cell. However, the apparent fluorescence lifetimes of 2.50 ns and 2.52 ns obtained using a 0.1 mm cell at 100 μM and 200 μM, respectively, are very similar to the intrinsic value of 2.5 ns. This indicates that reabsorption is negligible under these specific conditions (0.1 mm path length). In contrast, at 500 μM and 1000 μM, the decay signals differ clearly between the 0.1 mm and 1 mm cells. Furthermore, even with a 0.1 mm cell, the apparent fluorescence lifetimes at 500 μM (2.62 ns) and 1000 μM (2.70 ns) are longer than the intrinsic value of 2.5 ns.

To visualize this comparison, the decay signals at different concentrations are plotted in Figure S5. Signals obtained using a 10 mm path length cell were selected for 1 μM and 10 μM, while signals using the thinner 0.1 mm path length cell were selected for concentrations of 100 μM and above. As shown in Figure S5b, the four decay signals up to 200 μM are nearly identical. Conversely, the decay signals at 500 μM and 1000 μM are slightly slower than the others (Figure S5a). These results demonstrate that the effect of reabsorption is negligible up to 200 μM but becomes significant at 500 μM and 1000 μM under our experimental conditions. Similar results were obtained for eGFP, eYFP A206K, and eYFP using the same combinations of path length and concentration (Figure S5c-g).

For a quantitative assessment, the fraction of the excited-state population

produced by reabsorption f was estimated from the apparent fluorescence lifetimes at different concentrations. Figure S6 shows the calculated decay profiles using a single exponential function with the intrinsic fluorescence lifetime of eGFP A206K. The calculated decay profile was fitted using eq S2, and the residuals are shown at the top of each panel. The residuals are significantly larger for 500 μM and 1000 μM (Figure S6d, e) compared to those for 10 μM, 100 μM, and 200 μM (Figure S6a, b, c). This indicates a significant reabsorption contribution at 500 μM and 1000 μM. Although the estimated f values of 5.7% and 8.0% for 500 μM and 1000 μM, respectively, are relatively small, this reabsorption contribution is likely sufficient to distort the anisotropy decay signals. Importantly, however, the reabsorption contribution is zero at $t = 0$, confirming that the $r(0)$ values remain unaffected by reabsorption at any concentration.

Based on the above discussion, we conclude that under the experimental conditions employed in this paper, anisotropy signals at concentrations up to 200 μM provide both accurate $r(0)$ values and correct time-dependent behavior. At 500 μM and above, only the $r(0)$ values are accurately determined. In our previous study,[6] all anisotropy measurements were performed using cells with a path length of 10 mm. The anisotropy decays of eYFP A206K at 100 μM and 200 μM were fitted with a single exponential function, yielding decay constants of 11.3 ns and 10.4 ns, respectively. These faster decay rates compared to the present study (14.5 ns and 13.4 ns, respectively) indicate that depolarization due to reabsorption occurred under the conditions used in our previous work. This conclusion is further supported by the fact that the $r(0)$ values in the previous and present studies are very similar.

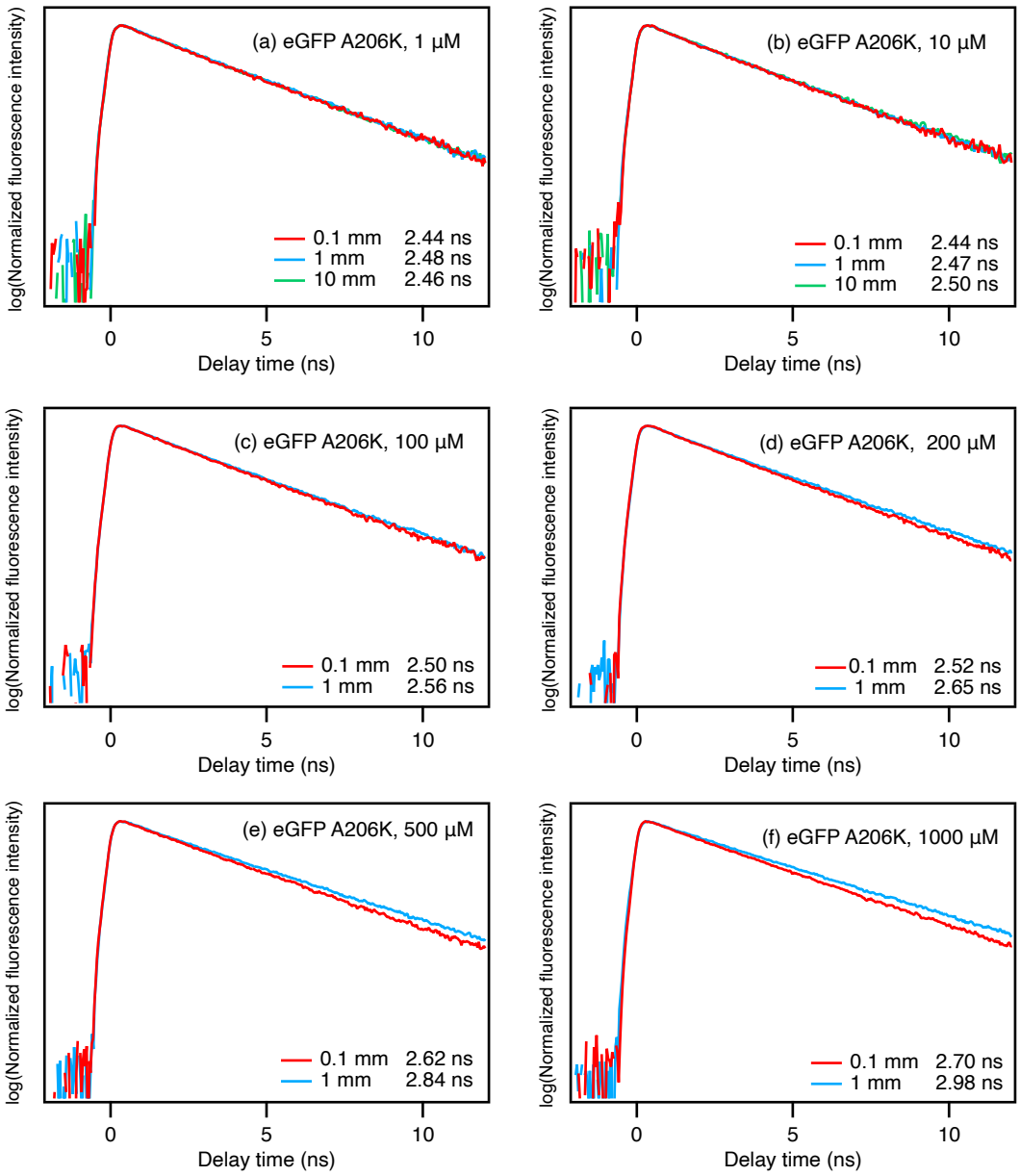

Figure S4. Time-resolved fluorescence decay signals of eGFP A206K measured at different concentrations using cells with different path lengths under magic-angle conditions (excitation: 500 nm; emission: 520–580 nm). The apparent fluorescence lifetimes, τ_{app}, were determined using eq S3 and are shown in each panel.

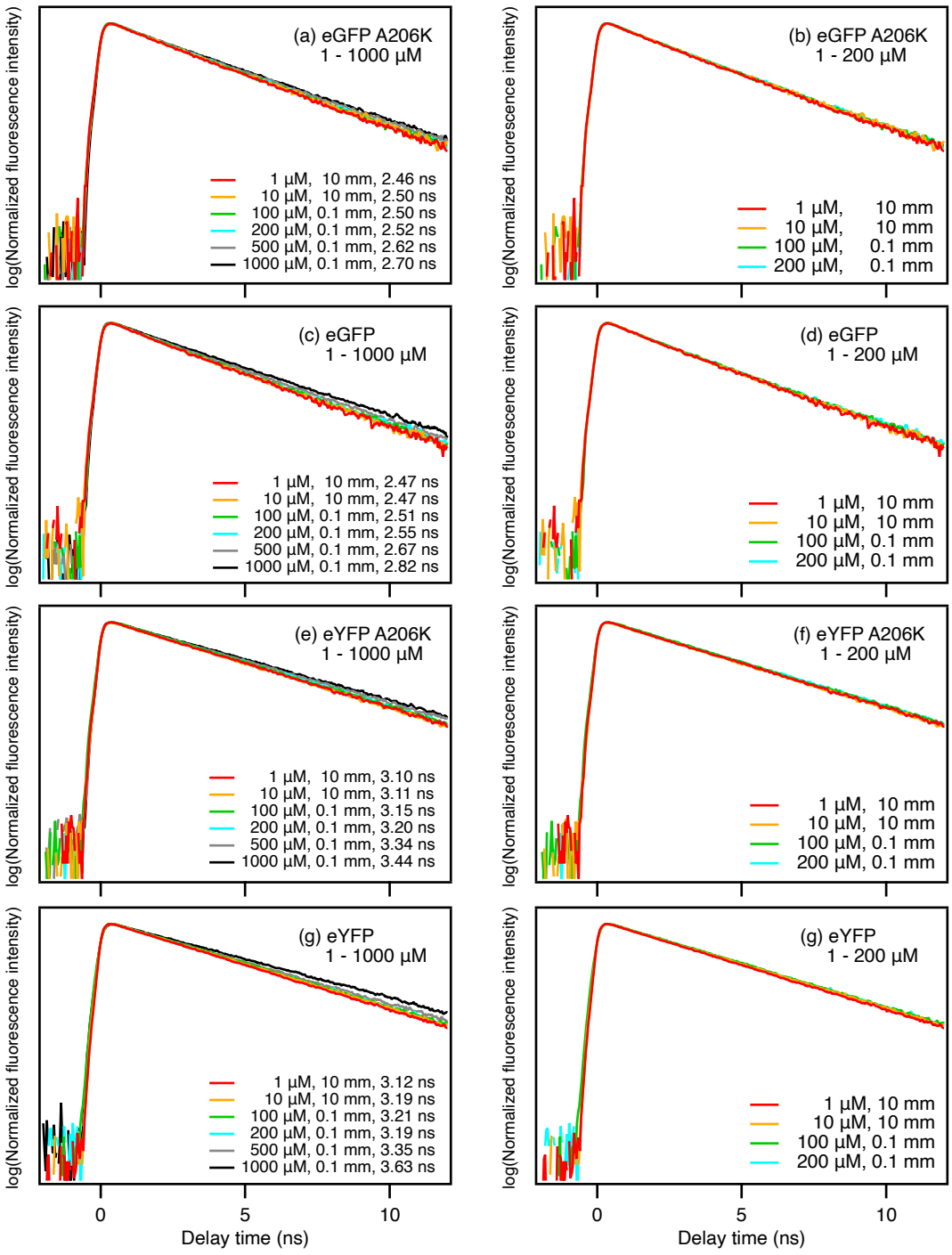

Figure S5. Time-resolved fluorescence decay signals of eGFP A206K, eGFP, eYFP A206K, and eYFP at different concentrations. The left and right panels show concentration ranges of 1–1000 µM and 1–200 µM, respectively. The path lengths and apparent fluorescence lifetimes, τ_{app}, are shown in each panel.

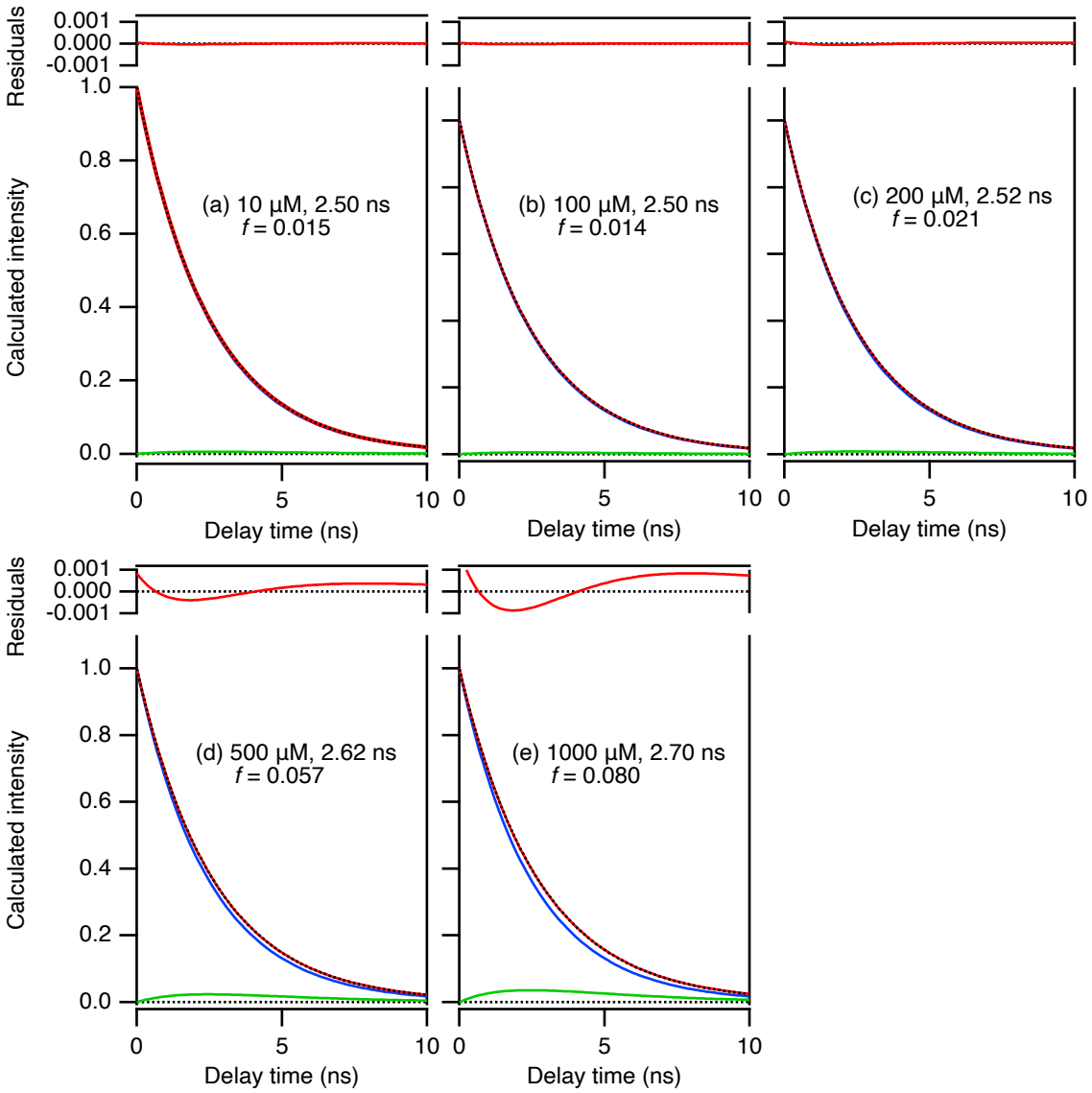

Figure S6. Calculated decay profiles generated using a single exponential function (red lines) based on the intrinsic fluorescence lifetime of eGFP A206K (Figure S5a). The apparent fluorescence lifetimes are indicated in each panel. The calculated profiles were fitted using eq S2 (black dotted lines). The intrinsic fluorescence lifetime, τ, is 2.46 ns (determined at 1 µM). The contributions from direct excitation (blue lines) and reabsorption (green lines) are plotted separately. The residuals are shown in the upper panels. The fraction of the excited-state population produced by reabsorption, f, is shown in each panel.

SI-5. pH dependence of fluorescence anisotropy curves of eGFP and eYFP.

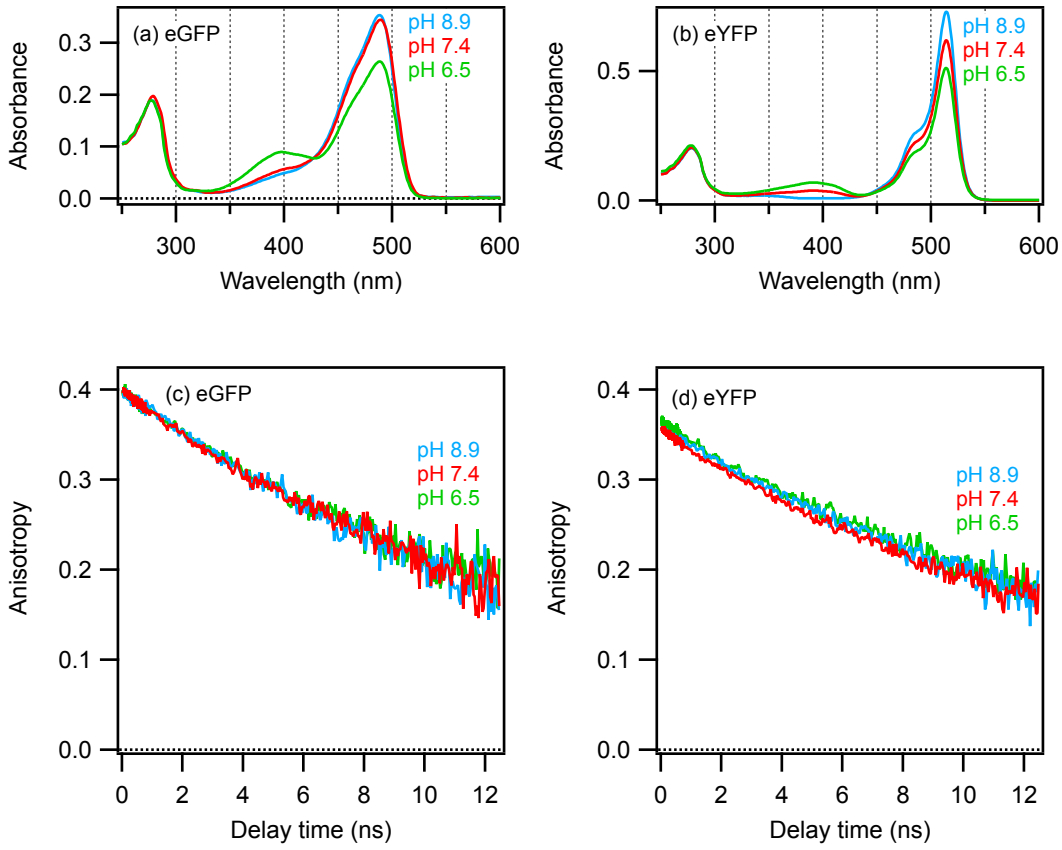

Figure S7. pH dependence of (a, b) absorption spectra and (c, d) fluorescence anisotropy decay curves for (a, c) eGFP and (b, d) eYFP. The excitation wavelengths were 500 nm for eGFP and 520 nm for eYFP. Fluorescence signals were collected over 520–580 nm for eGFP and 540–620 nm for eYFP. All measurements were performed in PBS at a protein concentration of 10 μM.

SI-6. Observed and calculated fluorescence anisotropy curves.

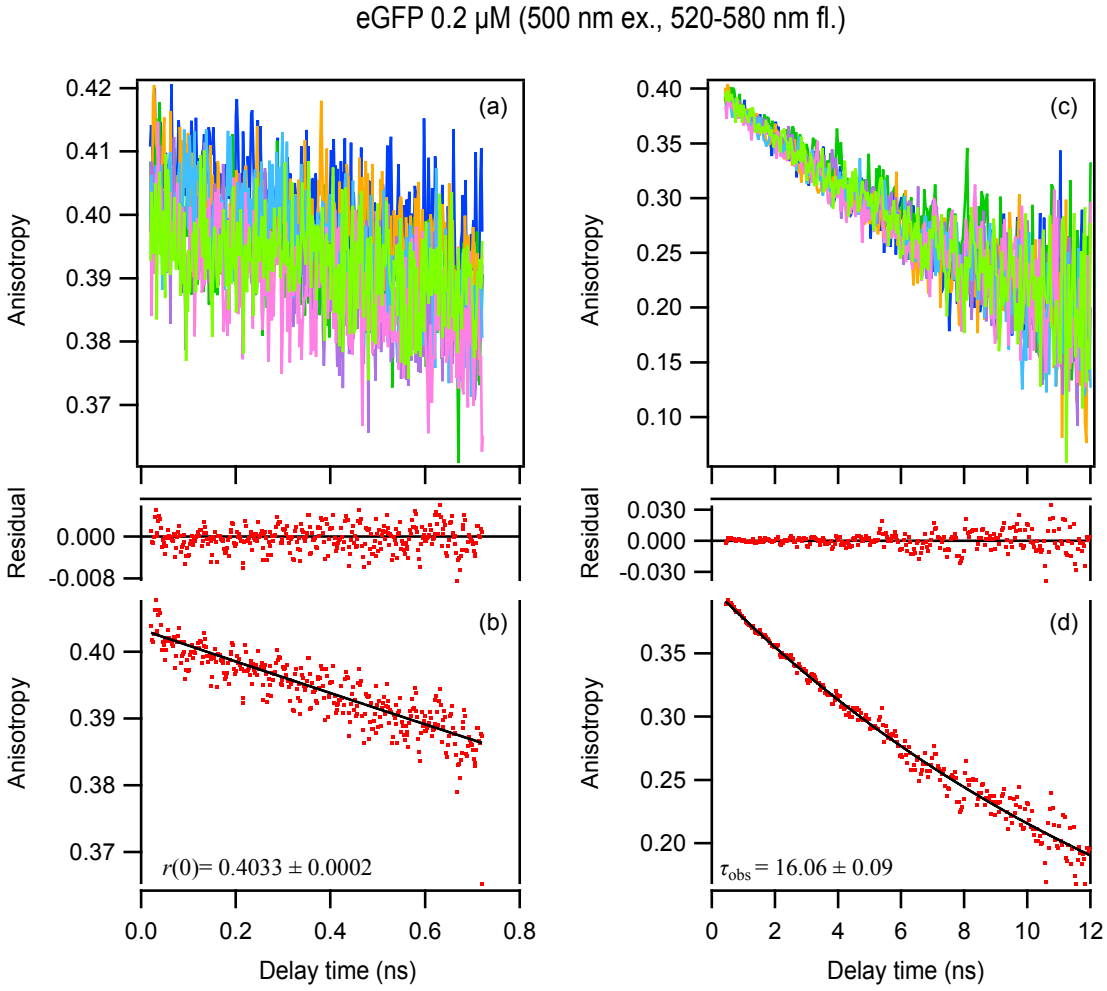

Figure S8. Superposition of fluorescence anisotropy decay curves from (a) 1-ns range (7 accumulations) and (c) 20-ns range (7 accumulations) measurements of 0.2 μM eGFP (PBS, pH 7.4). The corresponding averages are shown in (b) and (d), respectively. The excitation wavelength was 500 nm, and the fluorescence was collected over 520–580 nm. The *G*-factor was 0.990 for both 1-ns and 20-ns range measurements. The average curves were separately fitted using a single-exponential function (eq 7), and the fitting curves and residuals are also plotted. The anisotropy value at time 0, $r(0)$, was determined from the 1-ns range measurements, while the observed decay constant, τ_{obs}, was determined from the 20-ns range measurements. The obtained parameters with estimate of fitting errors are shown in each panel.

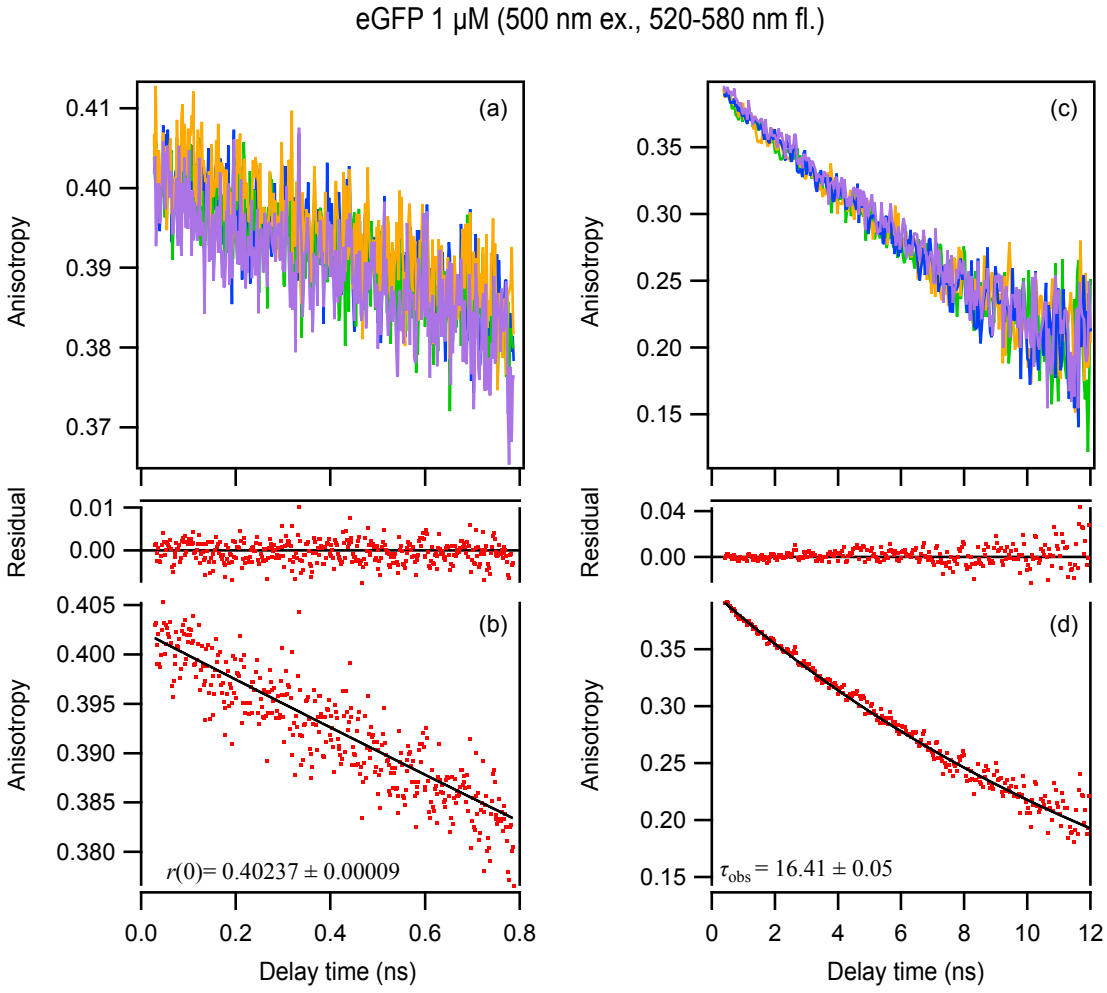

Figure S9. Superposition of fluorescence anisotropy decay curves from (a) 1-ns range (4 accumulations) and (c) 20-ns range (4 accumulations) measurements of 1 μM eGFP (PBS, pH 7.4). The corresponding averages are shown in (b) and (d), respectively. The excitation wavelength was 500 nm, and the fluorescence was collected over 520–580 nm. The *G*-factor was 0.972 for both 1-ns and 20-ns range measurements. The average curves were separately fitted using a single-exponential function (eq 7), and the fitting curves and residuals are also plotted. The anisotropy value at time 0, $r(0)$, was determined from the 1-ns range measurements, while the observed decay constant, τ_{obs}, was determined from the 20-ns range measurements. The obtained parameters with estimate of fitting errors are shown in each panel.

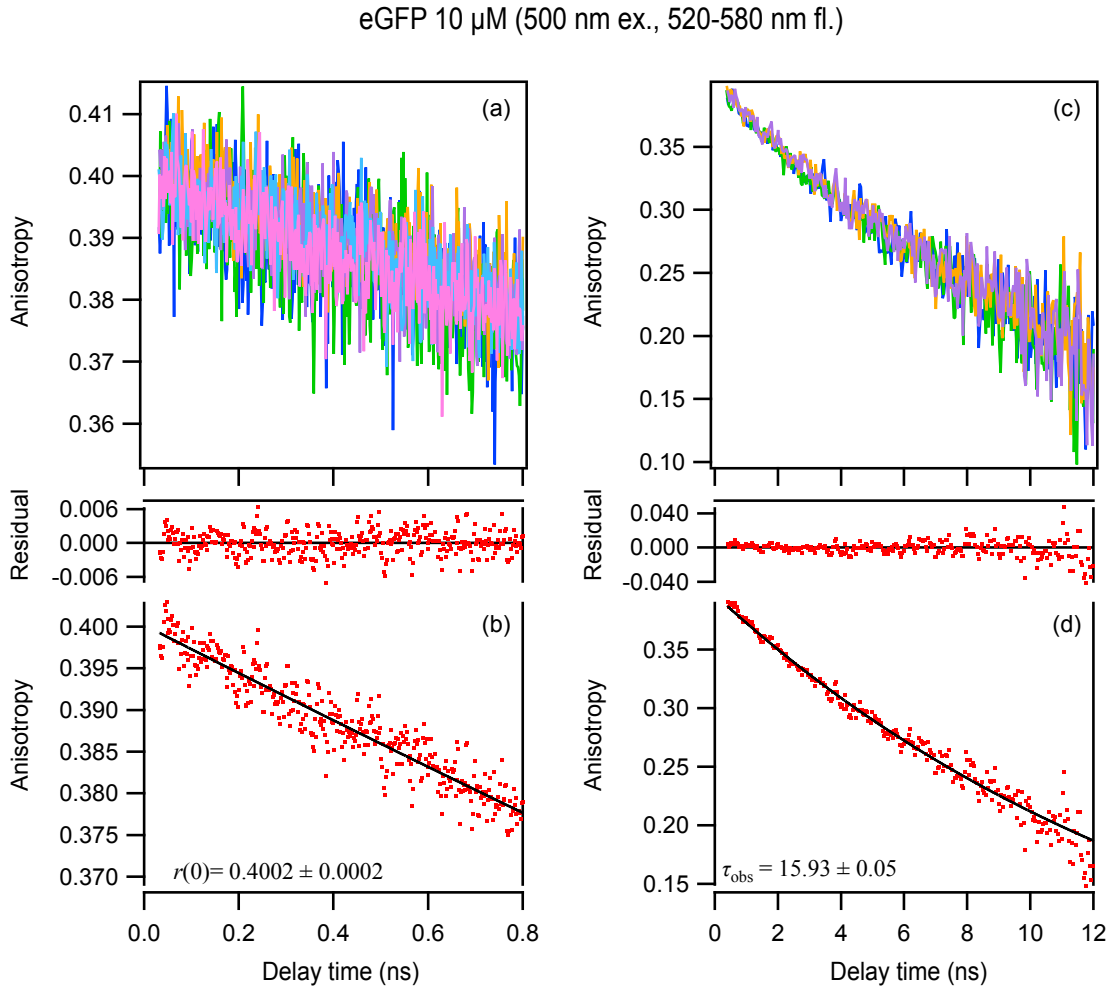

Figure S10. Superposition of fluorescence anisotropy decay curves from (a) 1-ns range (6 accumulations) and (c) 20-ns range (4 accumulations) measurements of 10 μM eGFP (PBS, pH 7.4). The corresponding averages are shown in (b) and (d), respectively. The excitation wavelength was 500 nm, and the fluorescence was collected over 520–580 nm. The *G*-factor was 0.972 for both 1-ns and 20-ns range measurements. The average curves were separately fitted using a single-exponential function (eq 7), and the fitting curves and residuals are also plotted. The anisotropy value at time 0, $r(0)$, was determined from the 1-ns range measurements, while the observed decay constant, τ_{obs}, was determined from the 20-ns range measurements. The obtained parameters with estimate of fitting errors are shown in each panel.

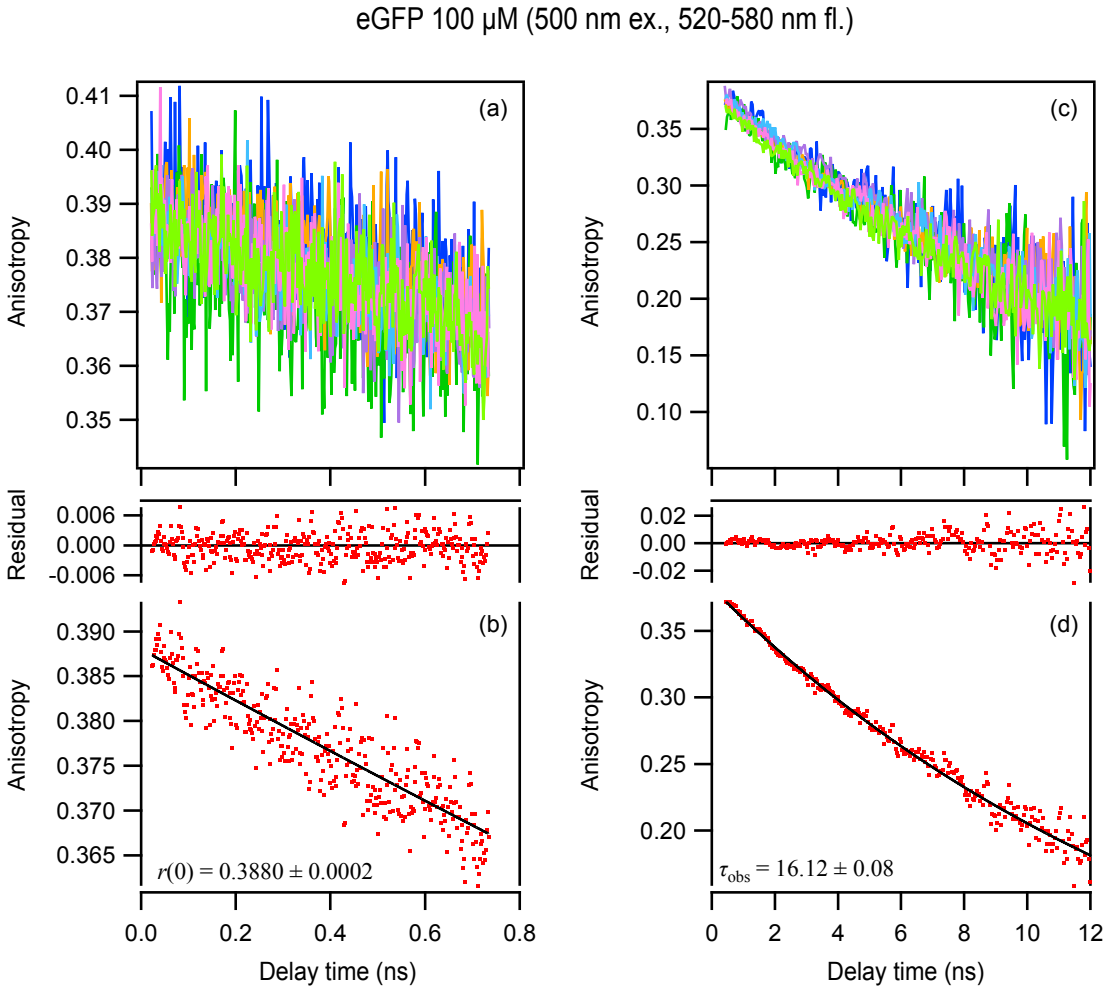

Figure S11. Superposition of fluorescence anisotropy decay curves from (a) 1-ns range (7 accumulations) and (c) 20-ns range (7 accumulations) measurements of 100 μM eGFP (PBS, pH 7.4). The corresponding averages are shown in (b) and (d), respectively. The excitation wavelength was 500 nm, and the fluorescence was collected over 520–580 nm. The *G*-factor was 0.972 for both 1-ns and 20-ns range measurements. The average curves were separately fitted using a single-exponential function (eq 7), and the fitting curves and residuals are also plotted. The anisotropy value at time 0, $r(0)$, was determined from the 1-ns range measurements, while the observed decay constant, τ_{obs}, was determined from the 20-ns range measurements. The obtained parameters with estimate of fitting errors are shown in each panel.

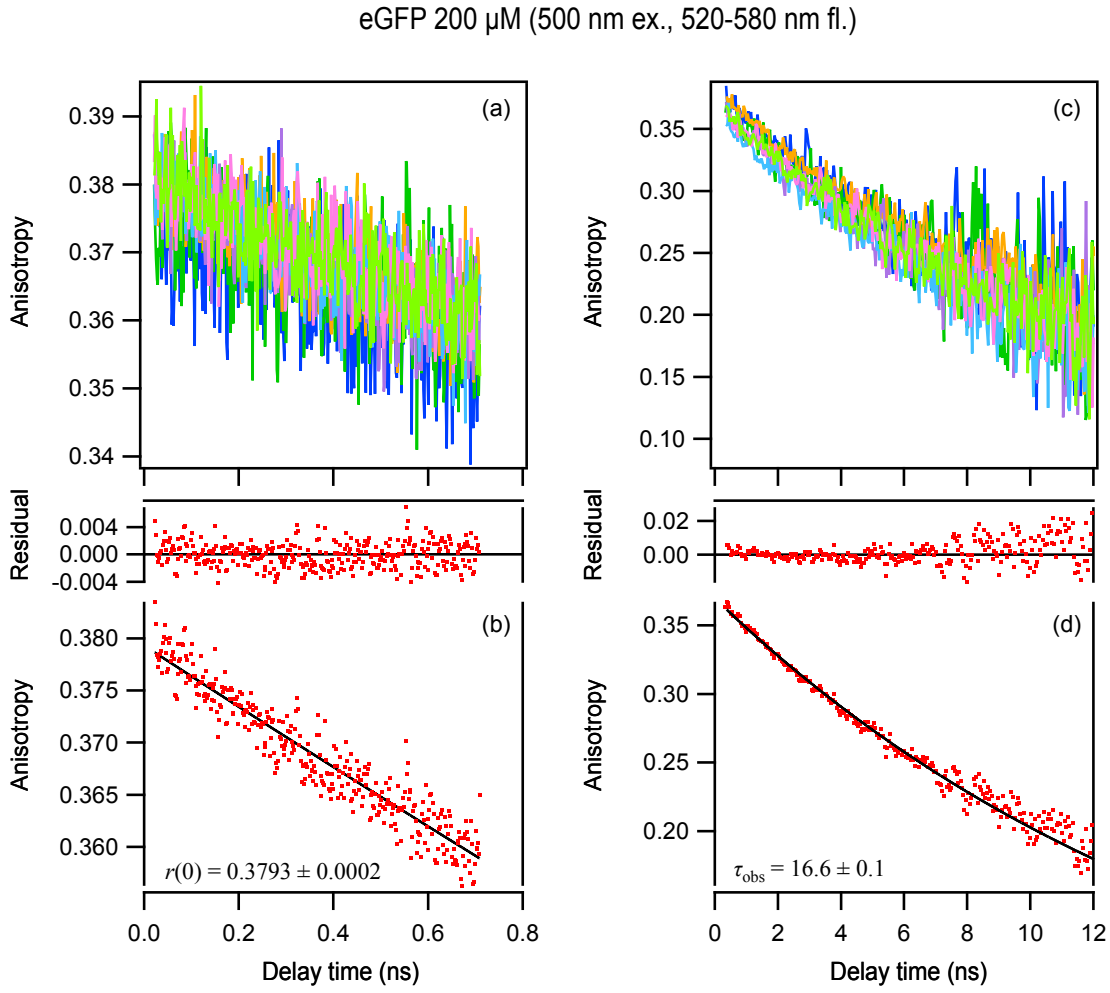

Figure S12. Superposition of fluorescence anisotropy decay curves from (a) 1-ns range (7 accumulations) and (c) 20-ns range (7 accumulations) measurements of 200 μM eGFP (PBS, pH 7.4). The corresponding averages are shown in (b) and (d), respectively. The excitation wavelength was 500 nm, and the fluorescence was collected over 520–580 nm. The *G*-factor was 0.972 for both 1-ns and 20-ns range measurements. The average curves were separately fitted using a single-exponential function (eq 7), and the fitting curves and residuals are also plotted. The anisotropy value at time 0, $r(0)$, was determined from the 1-ns range measurements, while the observed decay constant, τ_{obs}, was determined from the 20-ns range measurements. The obtained parameters with estimate of fitting errors are shown in each panel.

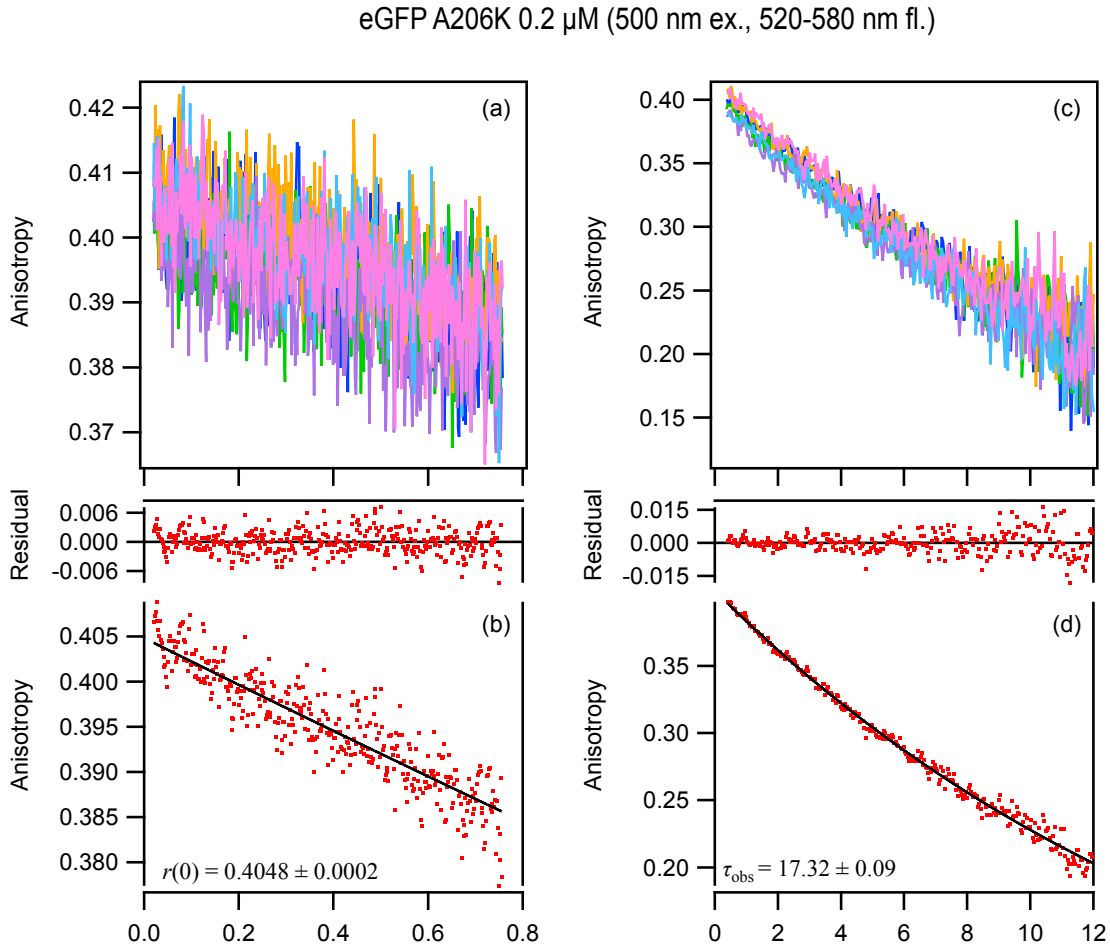

Figure S13. Superposition of fluorescence anisotropy decay curves from (a) 1-ns range (6 accumulations) and (c) 20-ns range (6 accumulations) measurements of 0.2 μM eGFP A206K (PBS, pH 7.4). The corresponding averages are shown in (b) and (d), respectively. The excitation wavelength was 500 nm, and the fluorescence was collected over 520–580 nm. The *G*-factors were 0.990 and 0.972 for the 1-ns and 20-ns range measurements, respectively. The average curves were separately fitted using a single-exponential function (eq 7), and the fitting curves and residuals are also plotted. The anisotropy value at time 0, $r(0)$, was determined from the 1-ns range measurements, while the observed decay constant, τ_{obs}, was determined from the 20-ns range measurements. The obtained parameters with estimate of fitting errors are shown in each panel.

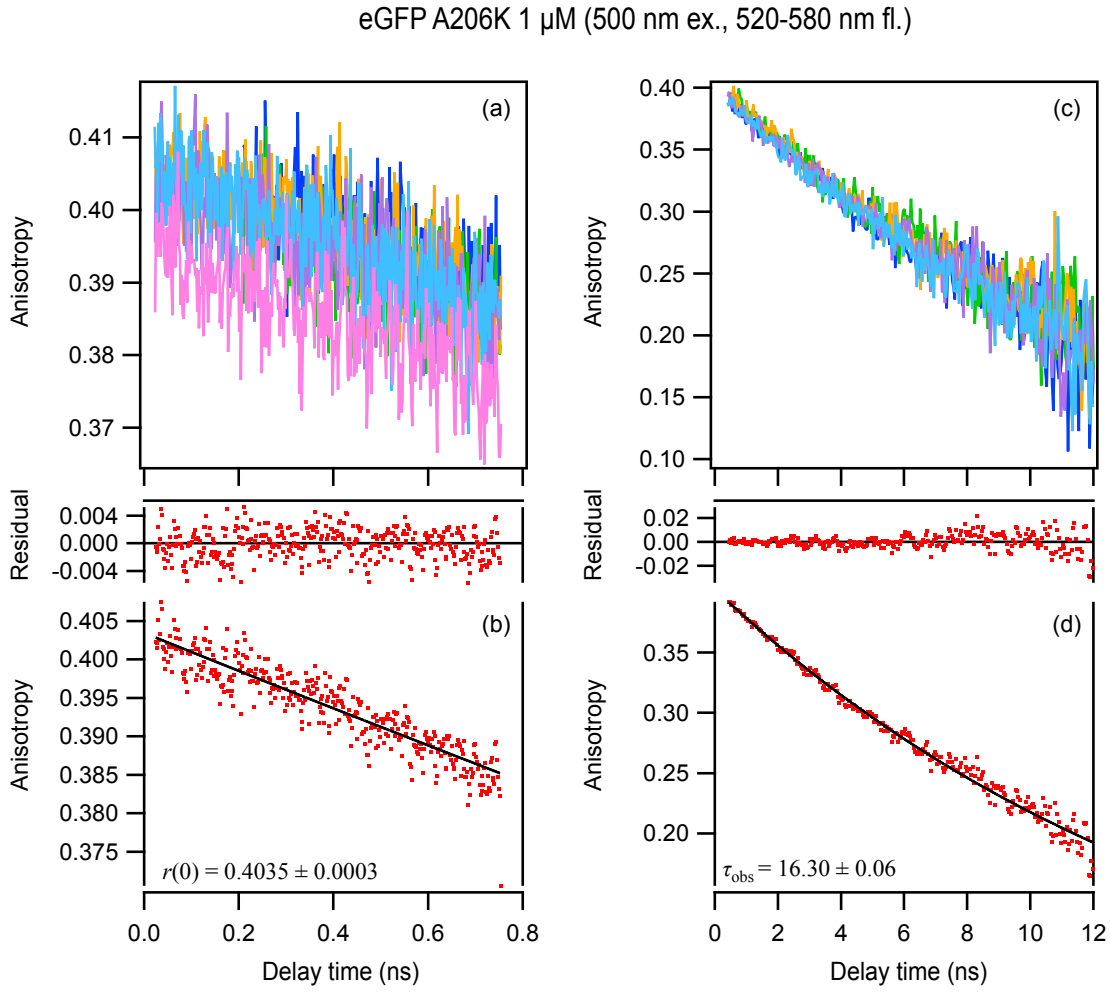

Figure S14. Superposition of fluorescence anisotropy decay curves from (a) 1-ns range (6 accumulations) and (c) 20-ns range (5 accumulations) measurements of 1 μM eGFP A206K (PBS, pH 7.4). The corresponding averages are shown in (b) and (d), respectively. The excitation wavelength was 500 nm, and the fluorescence was collected over 520–580 nm. The *G*-factors were 0.990 and 0.972 for the 1-ns and 20-ns range measurements, respectively. The average curves were separately fitted using a single-exponential function (eq 7), and the fitting curves and residuals are also plotted. The anisotropy value at time 0, $r(0)$, was determined from the 1-ns range measurements, while the observed decay constant, τ_{obs}, was determined from the 20-ns range measurements. The obtained parameters with estimate of fitting errors are shown in each panel.

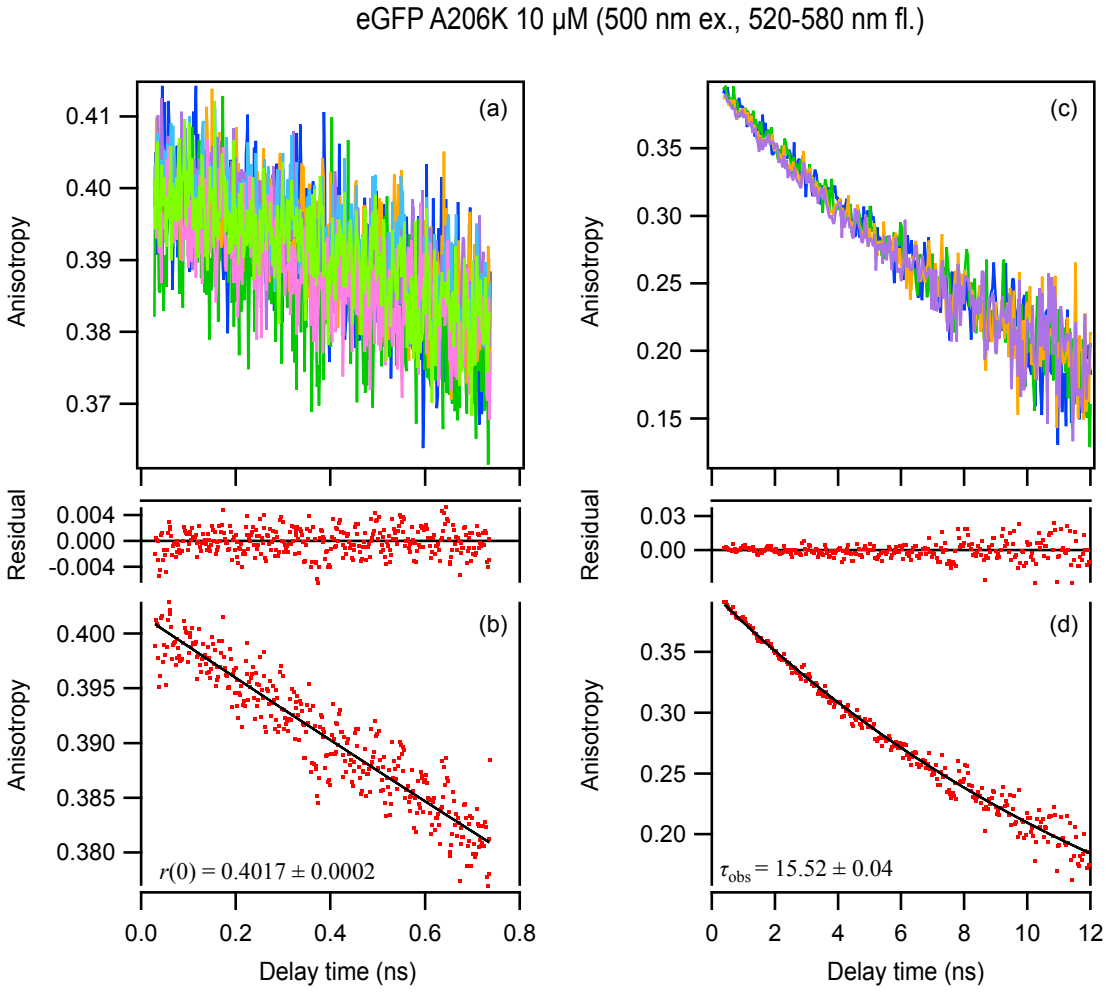

Figure S15. Superposition of fluorescence anisotropy decay curves from (a) 1-ns range (7 accumulations) and (c) 20-ns range (4 accumulations) measurements of 10 μM eGFP A206K (PBS, pH 7.4). The corresponding averages are shown in (b) and (d), respectively. The excitation wavelength was 500 nm, and the fluorescence was collected over 520–580 nm. The *G*-factors were 0.990 and 0.972 for the 1-ns and 20-ns range measurements, respectively. The average curves were separately fitted using a single-exponential function (eq 7), and the fitting curves and residuals are also plotted. The anisotropy value at time 0, $r(0)$, was determined from the 1-ns range measurements, while the observed decay constant, τ_{obs}, was determined from the 20-ns range measurements. The obtained parameters with estimate of fitting errors are shown in each panel.

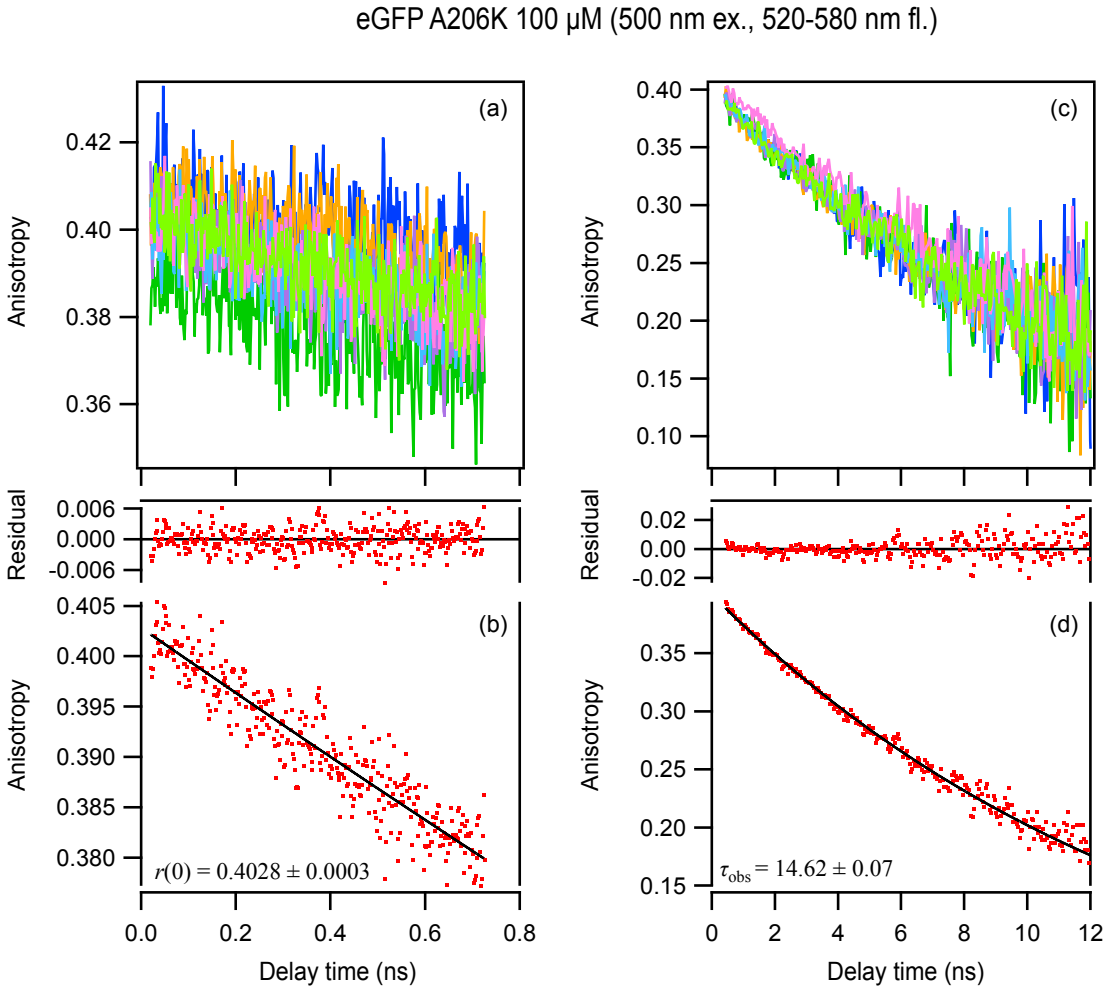

Figure S16. Superposition of fluorescence anisotropy decay curves from (a) 1-ns range (7 accumulations) and (c) 20-ns range (7 accumulations) measurements of 100 μM eGFP A206K (PBS, pH 7.4). The corresponding averages are shown in (b) and (d), respectively. The excitation wavelength was 500 nm, and the fluorescence was collected over 520–580 nm. The *G*-factor was 0.972 for both 1-ns and 20-ns range measurements. The average curves were separately fitted using a single-exponential function (eq 7), and the fitting curves and residuals are also plotted. The anisotropy value at time 0, $r(0)$, was determined from the 1-ns range measurements, while the observed decay constant, τ_{obs}, was determined from the 20-ns range measurements. The obtained parameters with estimate of fitting errors are shown in each panel.

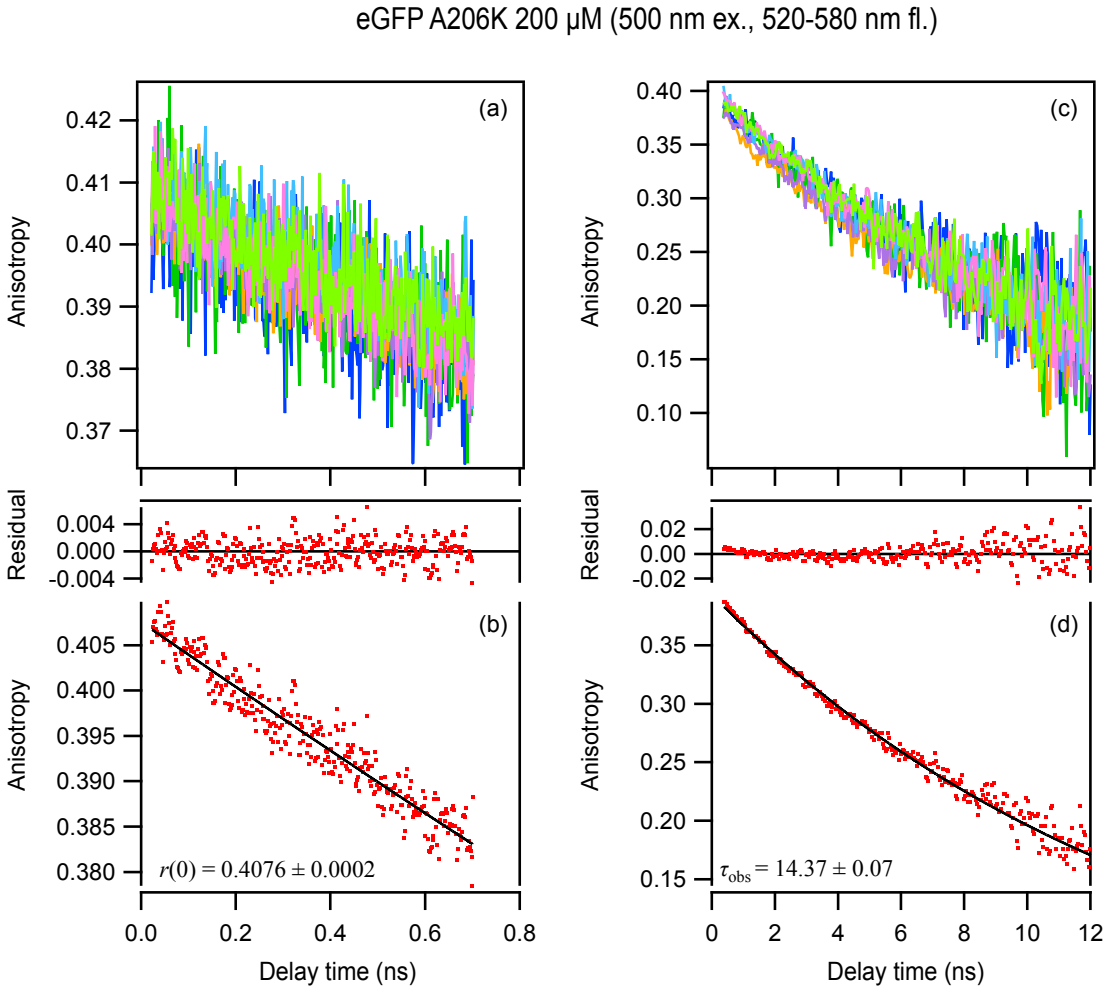

Figure S17. Superposition of fluorescence anisotropy decay curves from (a) 1-ns range (7 accumulations) and (c) 20-ns range (7 accumulations) measurements of 200 μM eGFP A206K (PBS, pH 7.4). The corresponding averages are shown in (b) and (d), respectively. The excitation wavelength was 500 nm, and the fluorescence was collected over 520–580 nm. The *G*-factor was 0.972 for both 1-ns and 20-ns range measurements. The average curves were separately fitted using a single-exponential function (eq 7), and the fitting curves and residuals are also plotted. The anisotropy value at time 0, $r(0)$, was determined from the 1-ns range measurements, while the observed decay constant, τ_{obs}, was determined from the 20-ns range measurements. The obtained parameters with estimate of fitting errors are shown in each panel.

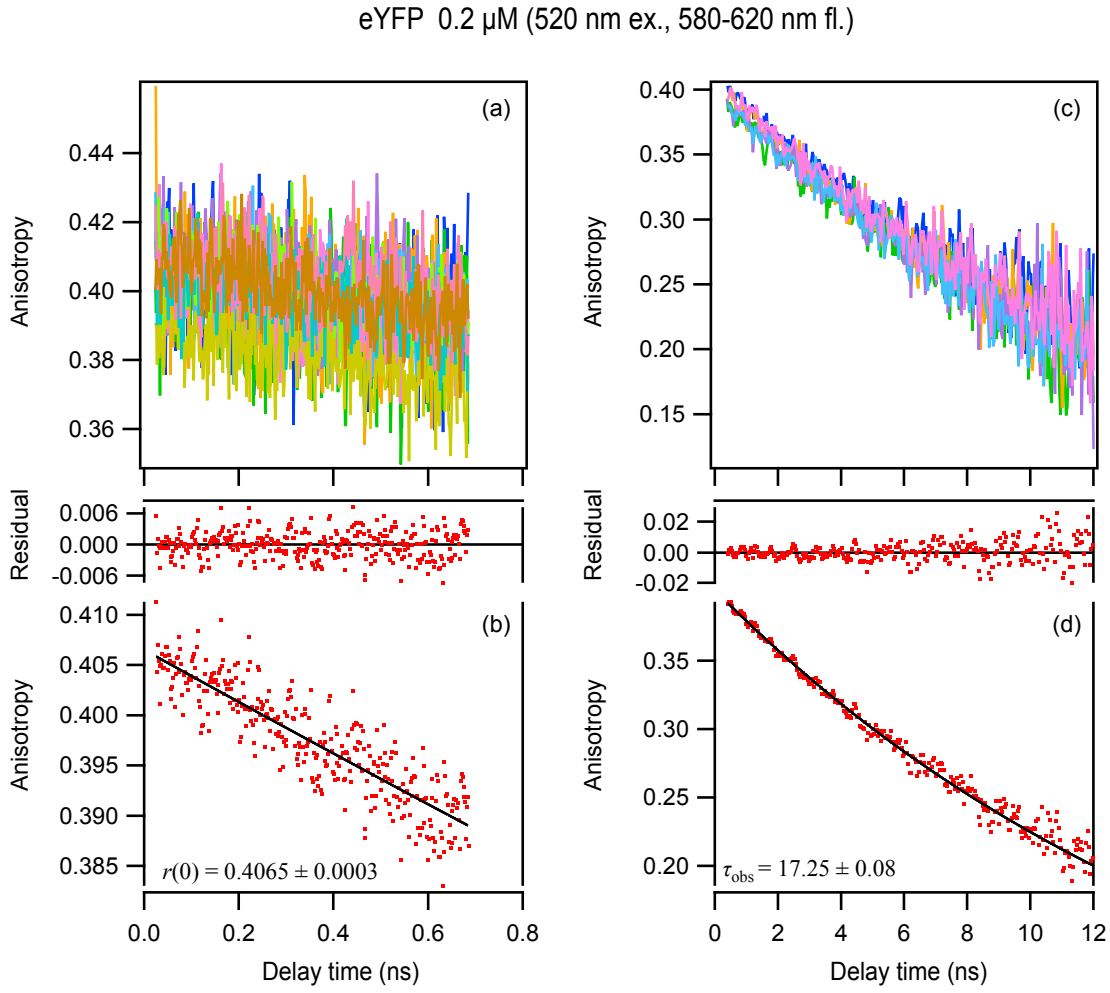

Figure S18. Superposition of fluorescence anisotropy decay curves from (a) 1-ns range (11 accumulations) and (c) 20-ns range (6 accumulations) measurements of 0.2 μM eYFP (PBS, pH 7.4). The corresponding averages are shown in (b) and (d), respectively. The excitation wavelength was 520 nm, and the fluorescence was collected over 540–620 nm. The *G*-factors were 0.997 and 0.968 for the 1-ns and 20-ns range measurements, respectively. The average curves were separately fitted using a single-exponential function (eq 7), and the fitting curves and residuals are also plotted. The anisotropy value at time 0, $r(0)$, was determined from the 1-ns range measurements, while the observed decay constant, τ_{obs}, was determined from the 20-ns range measurements. The obtained parameters with estimate of fitting errors are shown in each panel.

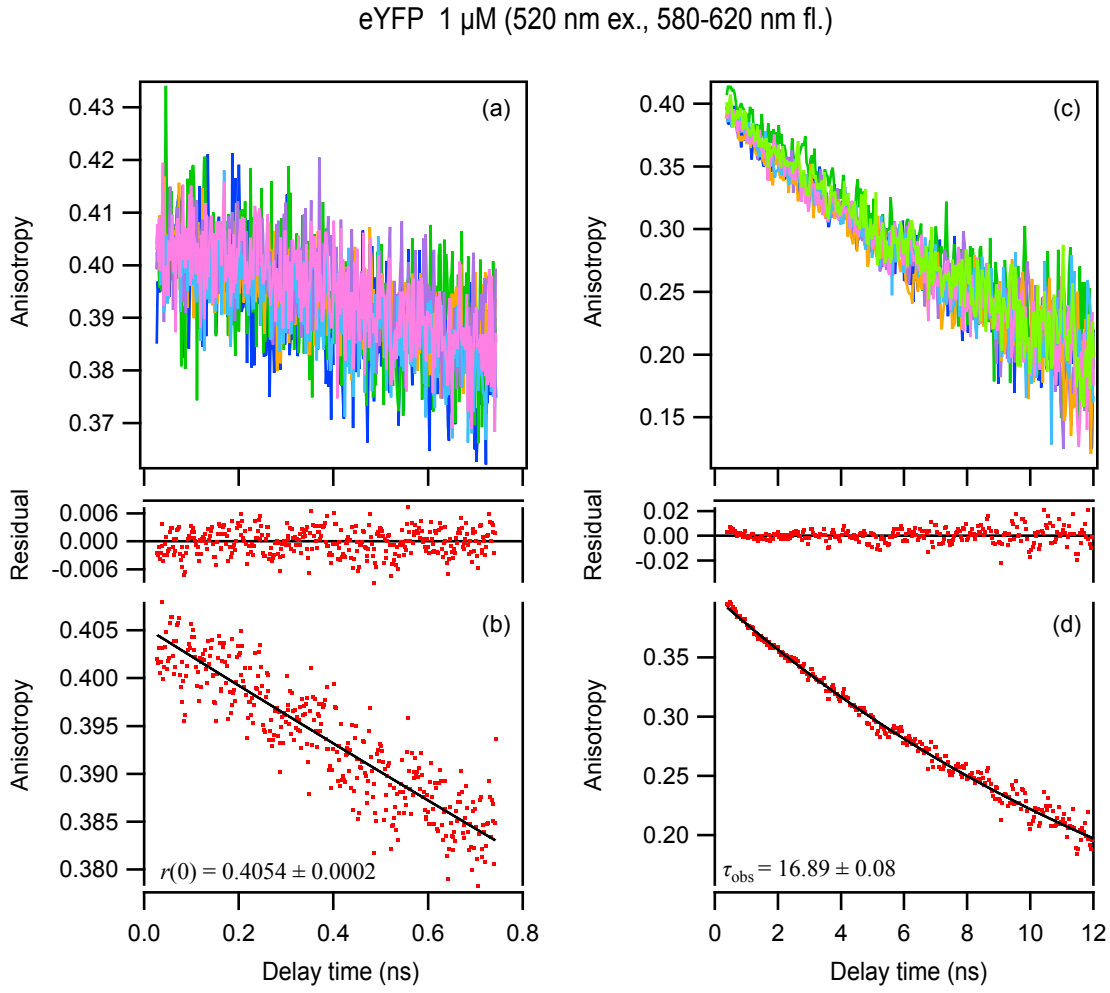

Figure S19. Superposition of fluorescence anisotropy decay curves from (a) 1-ns range (6 accumulations) and (c) 20-ns range (7 accumulations) measurements of 1 μM eYFP (PBS, pH 7.4). The corresponding averages are shown in (b) and (d), respectively. The excitation wavelength was 520 nm, and the fluorescence was collected over 540–620 nm. The *G*-factor was 0.997 for both 1-ns and 20-ns range measurements. The average curves were separately fitted using a single-exponential function (eq 7), and the fitting curves and residuals are also plotted. The anisotropy value at time 0, $r(0)$, was determined from the 1-ns range measurements, while the observed decay constant, τ_{obs}, was determined from the 20-ns range measurements. The obtained parameters with estimate of fitting errors are shown in each panel.

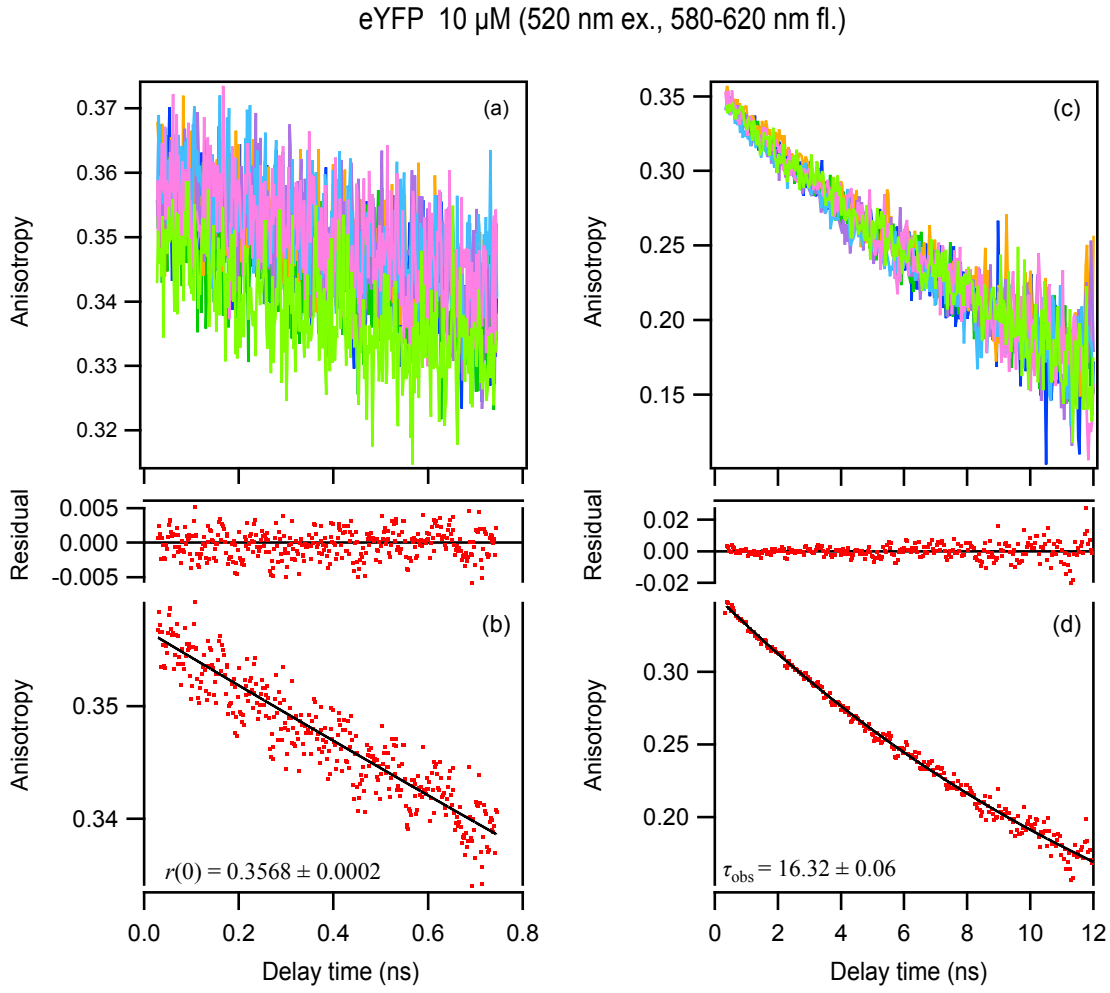

Figure S20. Superposition of fluorescence anisotropy decay curves from (a) 1-ns range (7 accumulations) and (c) 20-ns range (7 accumulations) measurements of 10 μM eYFP (PBS, pH 7.4). The corresponding averages are shown in (b) and (d), respectively. The excitation wavelength was 520 nm, and the fluorescence was collected over 540–620 nm. The *G*-factor was 0.997 for both 1-ns and 20-ns range measurements. The average curves were separately fitted using a single-exponential function (eq 7), and the fitting curves and residuals are also plotted. The anisotropy value at time 0, $r(0)$, was determined from the 1-ns range measurements, while the observed decay constant, τ_{obs}, was determined from the 20-ns range measurements. The obtained parameters with estimate of fitting errors are shown in each panel.

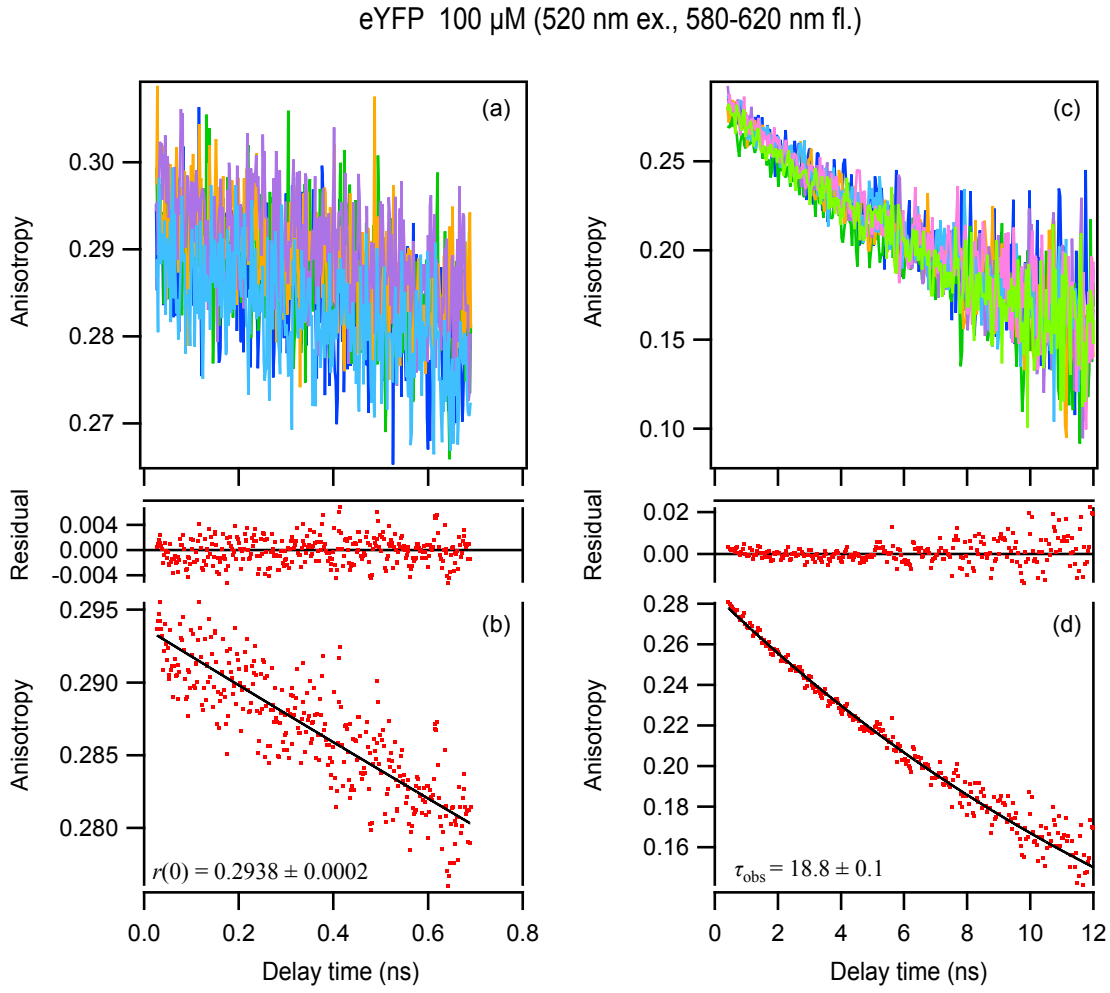

Figure S21. Superposition of fluorescence anisotropy decay curves from (a) 1-ns range (5 accumulations) and (c) 20-ns range (7 accumulations) measurements of 100 μM eYFP (PBS, pH 7.4). The corresponding averages are shown in (b) and (d), respectively. The excitation wavelength was 520 nm, and the fluorescence was collected over 540–620 nm. The *G*-factor was 1.000 for both 1-ns and 20-ns range measurements. The average curves were separately fitted using a single-exponential function (eq 7), and the fitting curves and residuals are also plotted. The anisotropy value at time 0, $r(0)$, was determined from the 1-ns range measurements, while the observed decay constant, τ_{obs}, was determined from the 20-ns range measurements. The obtained parameters with estimate of fitting errors are shown in each panel.

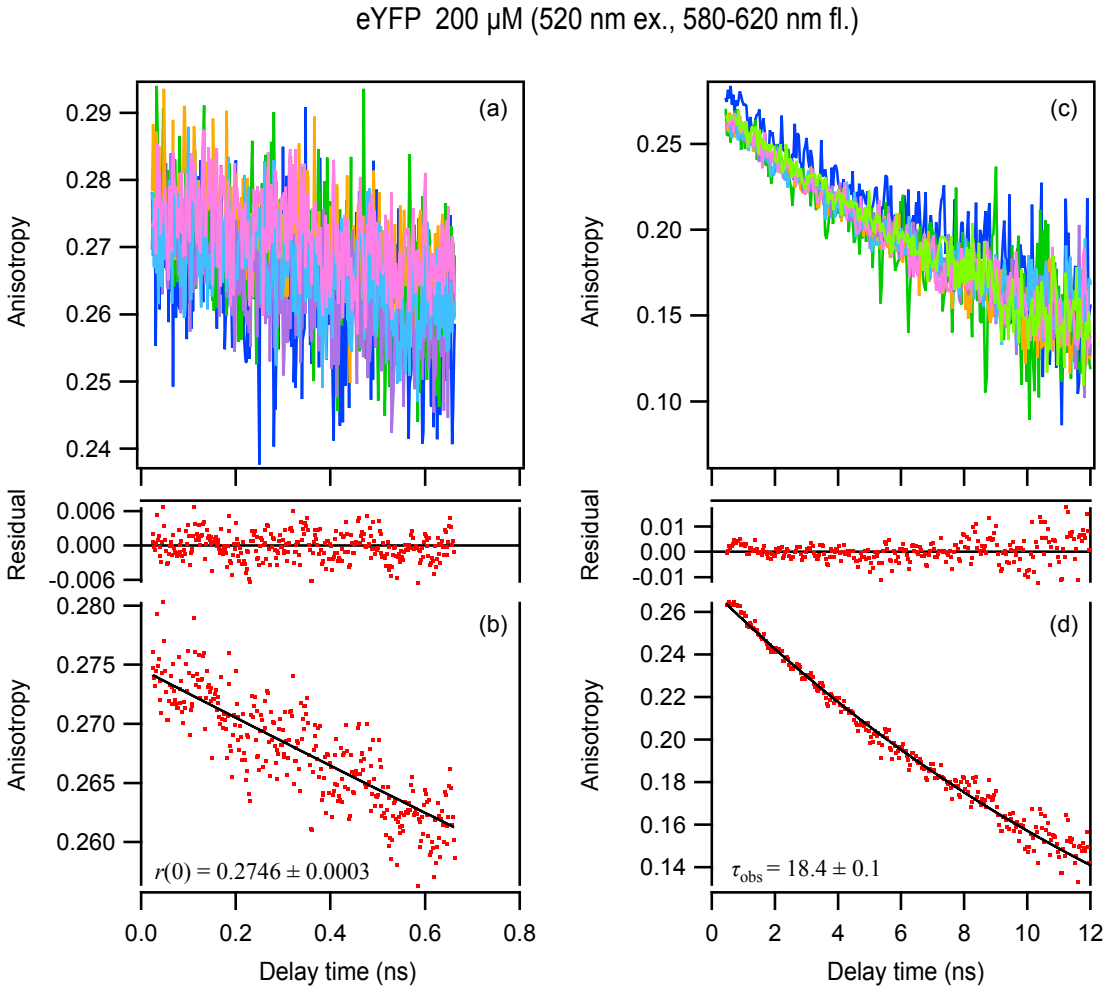

Figure S22. Superposition of fluorescence anisotropy decay curves from (a) 1-ns range (6 accumulations) and (c) 20-ns range (7 accumulations) measurements of 200 μM eYFP (PBS, pH 7.4). The corresponding averages are shown in (b) and (d), respectively. The excitation wavelength was 520 nm, and the fluorescence was collected over 540–620 nm. The *G*-factor was 0.992 for both 1-ns and 20-ns range measurements. The average curves were separately fitted using a single-exponential function (eq 7), and the fitting curves and residuals are also plotted. The anisotropy value at time 0, $r(0)$, was determined from the 1-ns range measurements, while the observed decay constant, τ_{obs}, was determined from the 20-ns range measurements. The obtained parameters with estimate of fitting errors are shown in each panel.

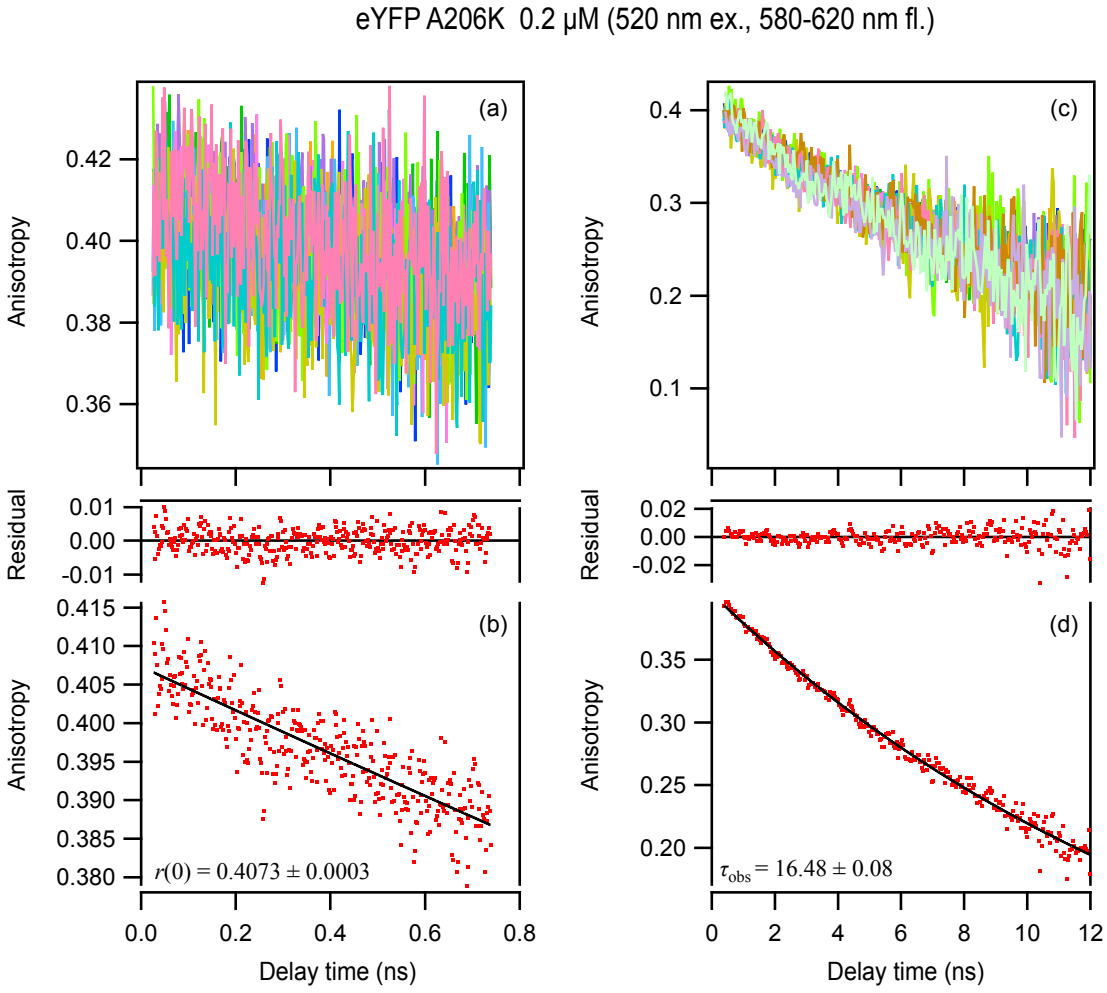

Figure S23. Superposition of fluorescence anisotropy decay curves from (a) 1-ns range (10 accumulations) and (c) 20-ns range (13 accumulations) measurements of 0.2 μM eYFP A206K (PBS, pH 7.4). The corresponding averages are shown in (b) and (d), respectively. The excitation wavelength was 520 nm, and the fluorescence was collected over 540–620 nm. The G-factor was 0.997 for the 1-ns range measurements, and 0.997 or 0.968 for the 20-ns range measurements. The average curves were separately fitted using a single-exponential function (eq 7), and the fitting curves and residuals are also plotted. The anisotropy value at time 0, $r(0)$, was determined from the 1-ns range measurements, while the observed decay constant, τ_{obs}, was determined from the 20-ns range measurements. The obtained parameters with estimate of fitting errors are shown in each panel.

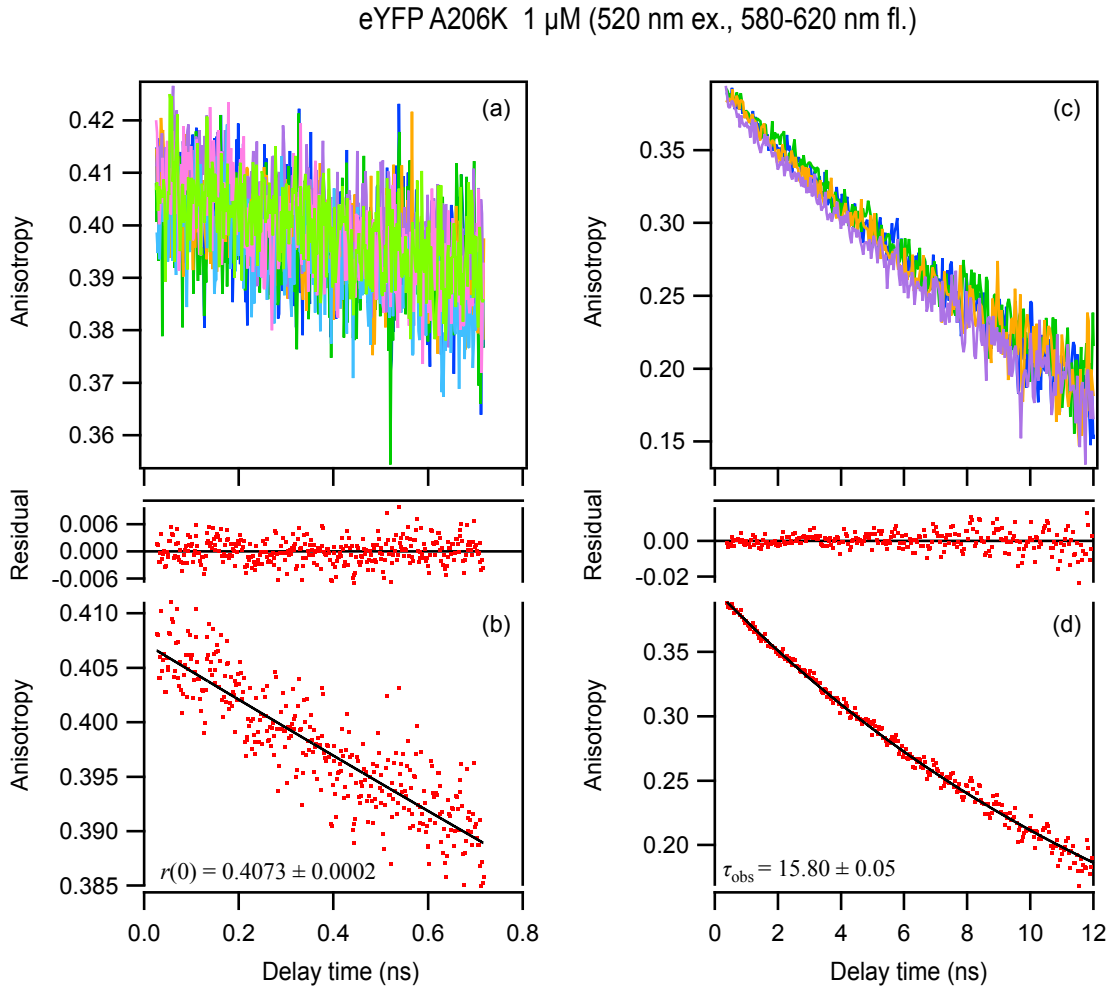

Figure S24. Superposition of fluorescence anisotropy decay curves from (a) 1-ns range (7 accumulations) and (c) 20-ns range (4 accumulations) measurements of 1 μM eYFP A206K (PBS, pH 7.4). The corresponding averages are shown in (b) and (d), respectively. The excitation wavelength was 520 nm, and the fluorescence was collected over 540–620 nm. The *G*-factor was 0.968 for both 1-ns and 20-ns range measurements. The average curves were separately fitted using a single-exponential function (eq 7), and the fitting curves and residuals are also plotted. The anisotropy value at time 0, $r(0)$, was determined from the 1-ns range measurements, while the observed decay constant, τ_{obs}, was determined from the 20-ns range measurements. The obtained parameters with estimate of fitting errors are shown in each panel.

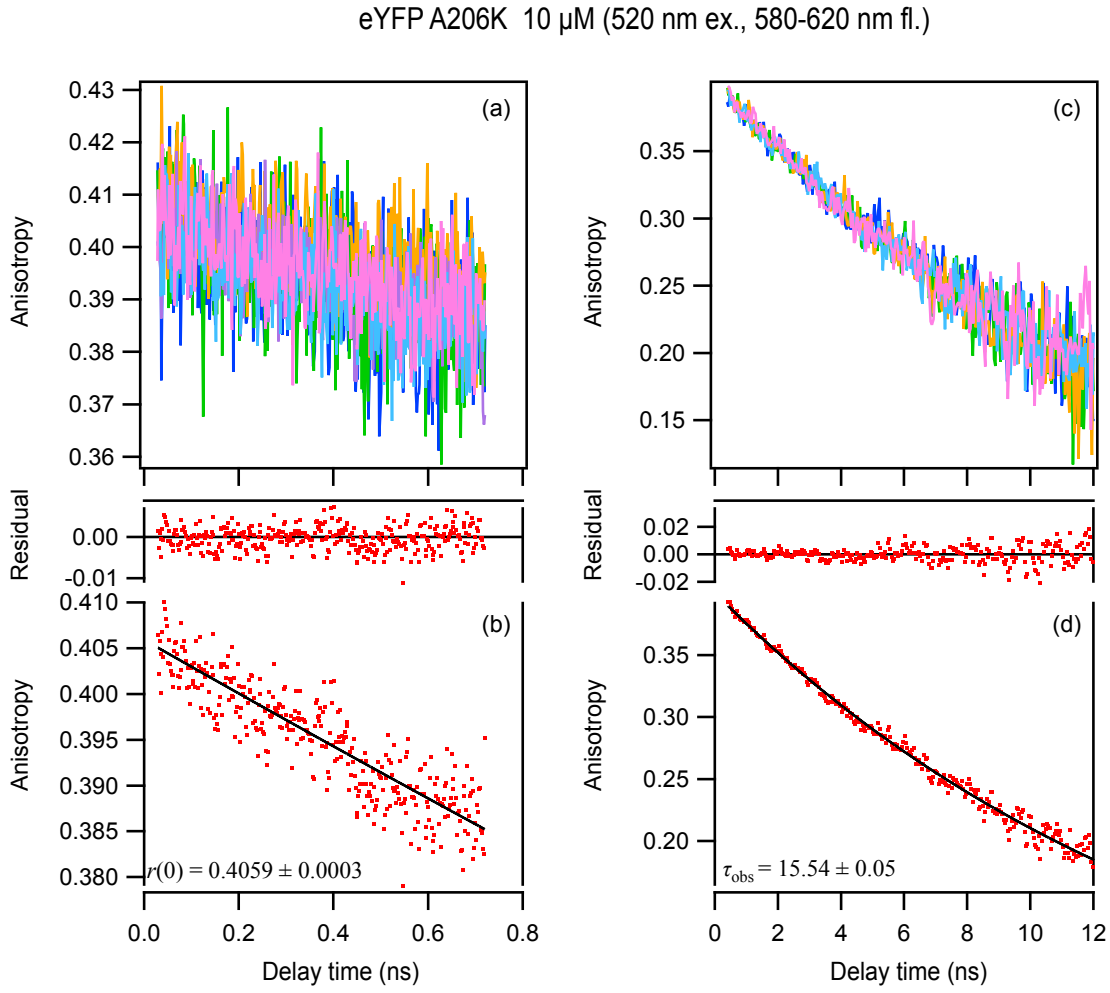

Figure S25. Superposition of fluorescence anisotropy decay curves from (a) 1-ns range (6 accumulations) and (c) 20-ns range (6 accumulations) measurements of 10 μM eYFP A206K (PBS, pH 7.4). The corresponding averages are shown in (b) and (d), respectively. The excitation wavelength was 520 nm, and the fluorescence was collected over 540–620 nm. The *G*-factor was 0.997 for both 1-ns and 20-ns range measurements. The average curves were separately fitted using a single-exponential function (eq 7), and the fitting curves and residuals are also plotted. The anisotropy value at time 0, $r(0)$, was determined from the 1-ns range measurements, while the observed decay constant, τ_{obs}, was determined from the 20-ns range measurements. The obtained parameters with estimate of fitting errors are shown in each panel.

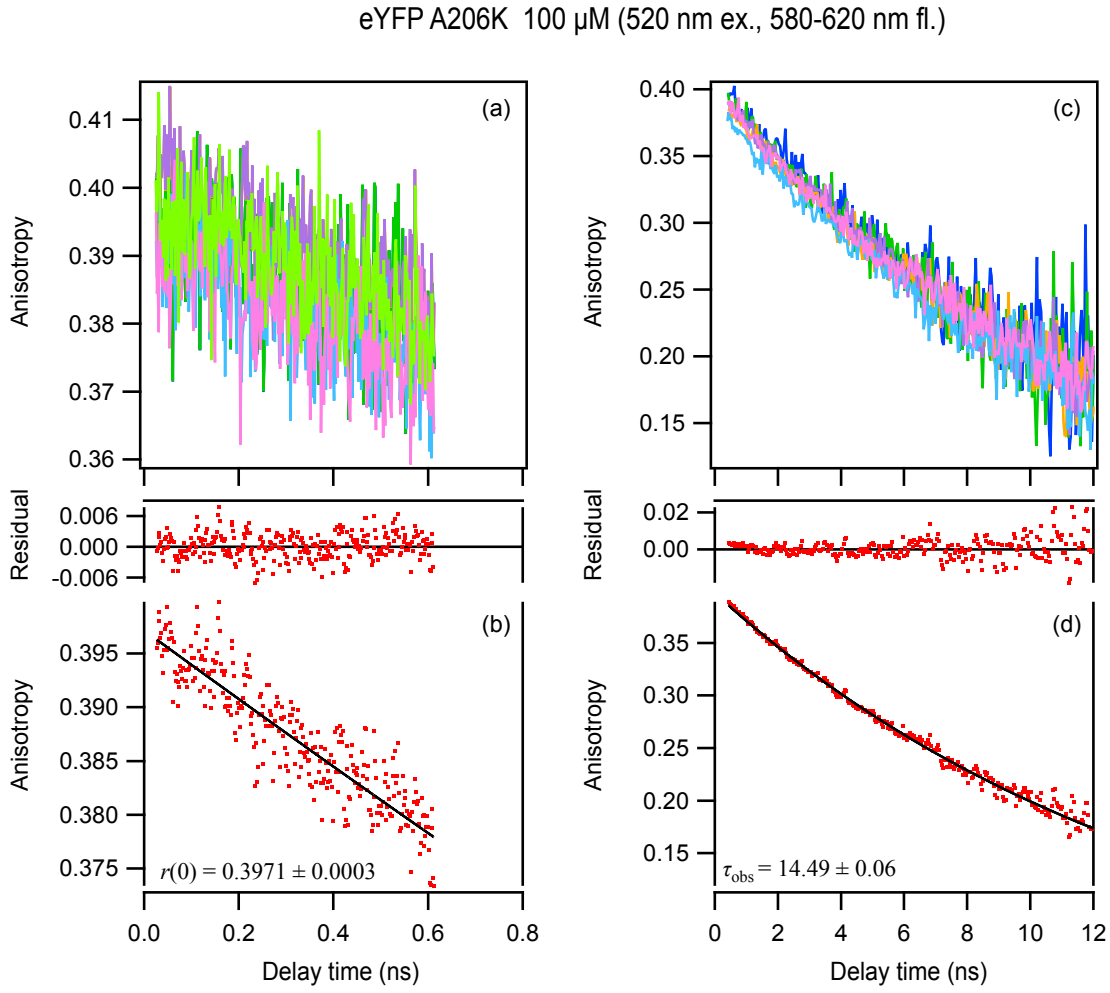

Figure S26. Superposition of fluorescence anisotropy decay curves from (a) 1-ns range (7 accumulations) and (c) 20-ns range (6 accumulations) measurements of 100 µM eYFP A206K (PBS, pH 7.4). The corresponding averages are shown in (b) and (d), respectively. The excitation wavelength was 520 nm, and the fluorescence was collected over 540–620 nm. The *G*-factor was 1.000 for both 1-ns and 20-ns range measurements. The average curves were separately fitted using a single-exponential function (eq 7), and the fitting curves and residuals are also plotted. The anisotropy value at time 0, $r(0)$, was determined from the 1-ns range measurements, while the observed decay constant, τ_{obs}, was determined from the 20-ns range measurements. The obtained parameters with estimate of fitting errors are shown in each panel.

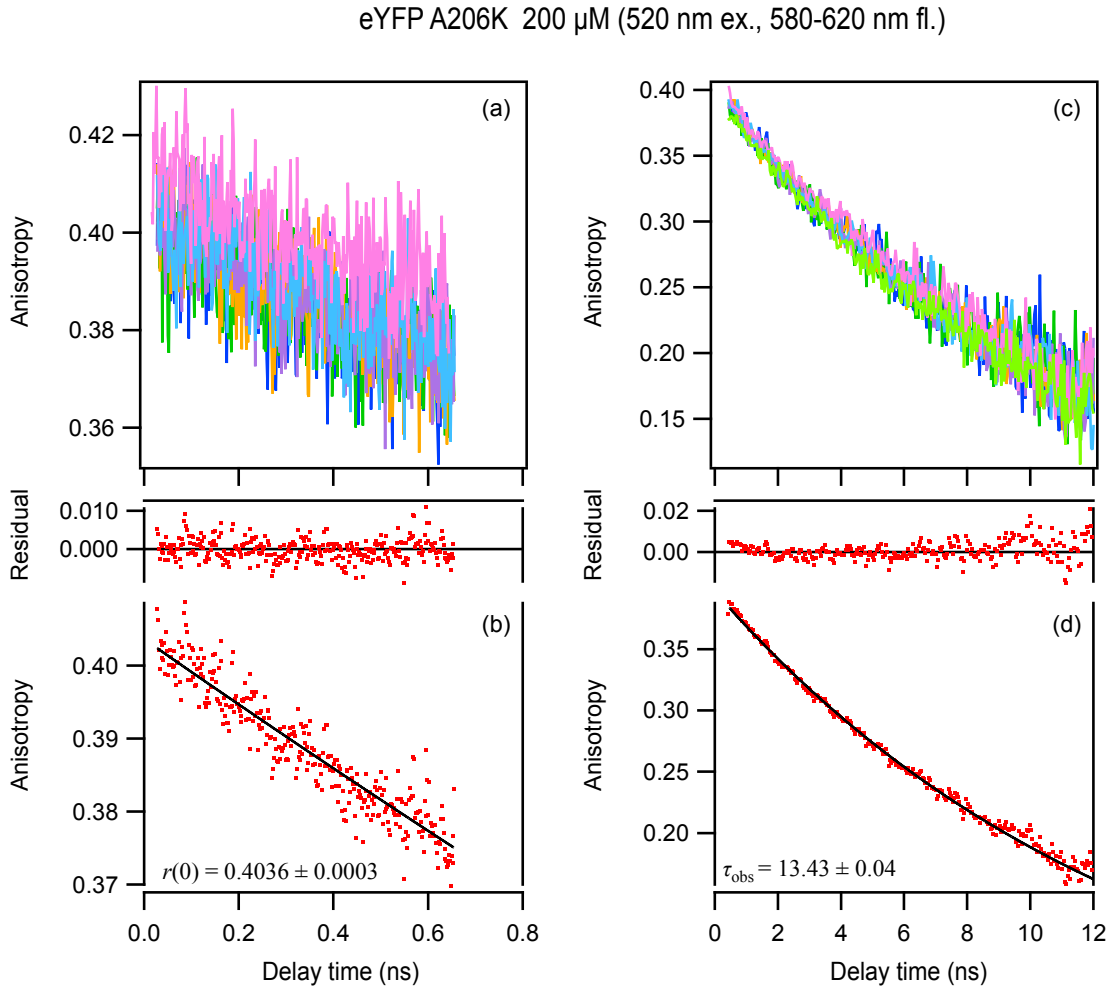

Figure S27. Superposition of fluorescence anisotropy decay curves from (a) 1-ns range (6 accumulations) and (c) 20-ns range (7 accumulations) measurements of 200 μM eYFP A206K (PBS, pH 7.4). The corresponding averages are shown in (b) and (d), respectively. The excitation wavelength was 520 nm, and the fluorescence was collected over 540–620 nm. The *G*-factor was 0.992 for both 1-ns and 20-ns range measurements. The average curves were separately fitted using a single-exponential function (eq 7), and the fitting curves and residuals are also plotted. The anisotropy value at time 0, $r(0)$, was determined from the 1-ns range measurements, while the observed decay constant, τ_{obs}, was determined from the 20-ns range measurements. The obtained parameters with estimate of fitting errors are shown in each panel.

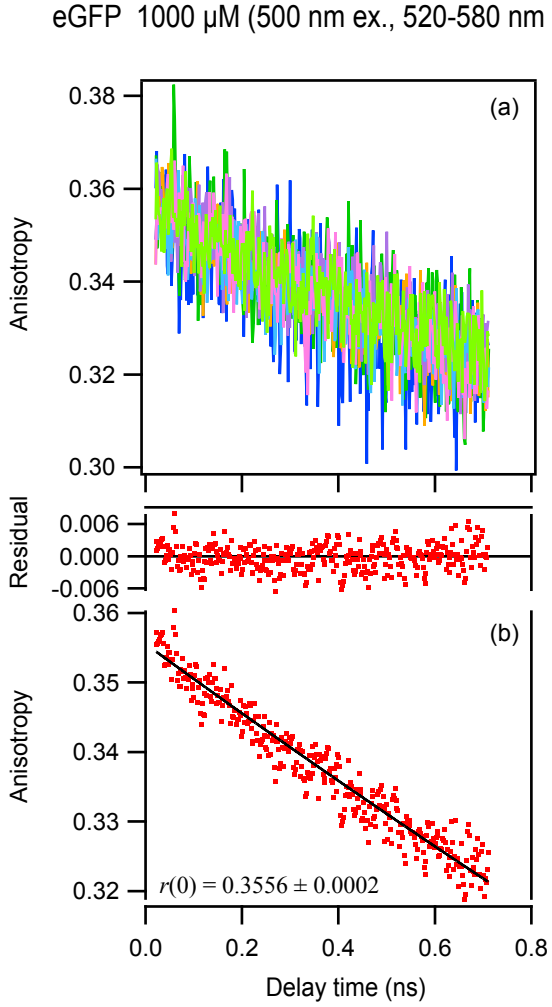

Figure S28. (a) Superposition of fluorescence anisotropy decay curves for 1-ns range measurements (7 accumulations) of 1000 μM eGFP (PBS, pH 7.4). The corresponding average is shown in (b). The excitation wavelength was 500 nm, and fluorescence was collected over 520–580 nm. The *G*-factor was 0.972. The average curve was fitted using a single-exponential function (eq 7), and the fitting curve and residuals are also plotted in (b). The anisotropy value at time 0, $r(0)$, with the standard error is shown in (b).

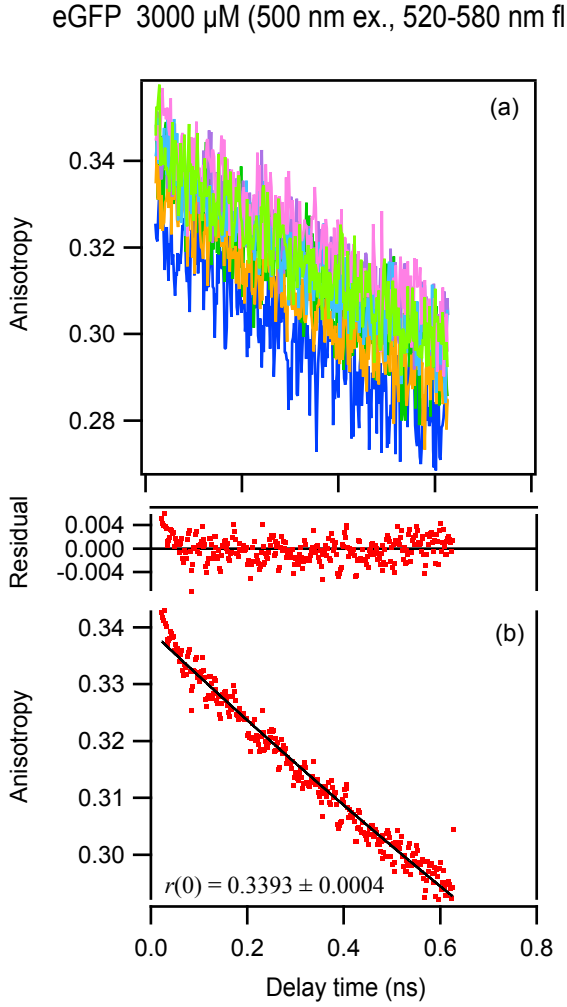

Figure S29. (a) Superposition of fluorescence anisotropy decay curves for 1-ns range measurements (7 accumulations) of 3000 μM eGFP (PBS, pH 7.4). The corresponding average is shown in (b). The excitation wavelength was 500 nm, and fluorescence was collected over 520–580 nm. The *G*-factor was 0.972. The average curve was fitted using a single-exponential function (eq 7), and the fitting curve and residuals are also plotted in (b). The anisotropy value at time 0, $r(0)$, with the standard error is shown in (b).

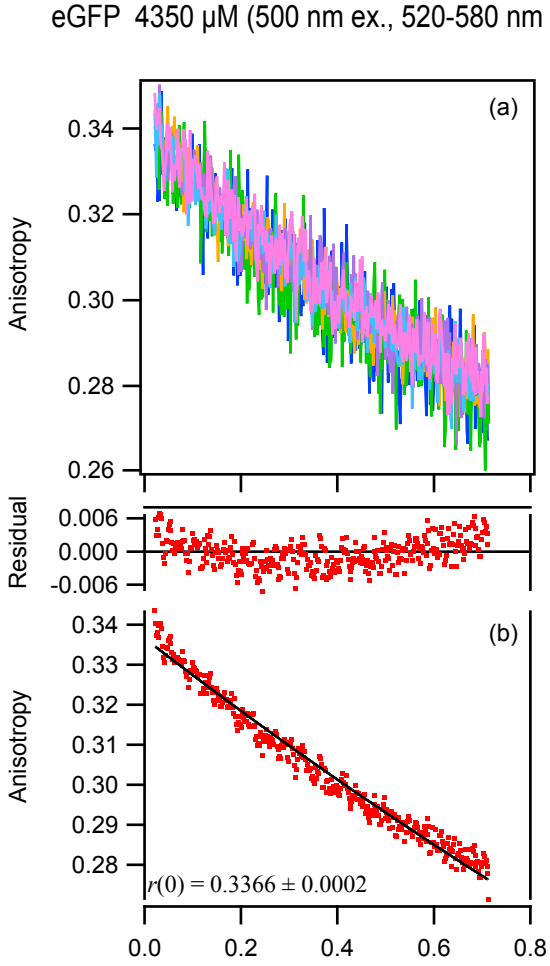

Figure S30. (a) Superposition of fluorescence anisotropy decay curves for 1-ns range measurements (6 accumulations) of 4350 µM eGFP (PBS, pH 7.4). The corresponding average is shown in (b). The excitation wavelength was 500 nm, and fluorescence was collected over 520–580 nm. The *G*-factor was 0.972. The average curve was fitted using a single-exponential function (eq 7), and the fitting curve and residuals are also plotted in (b). The anisotropy value at time 0, $r(0)$, with the standard error is shown in (b).

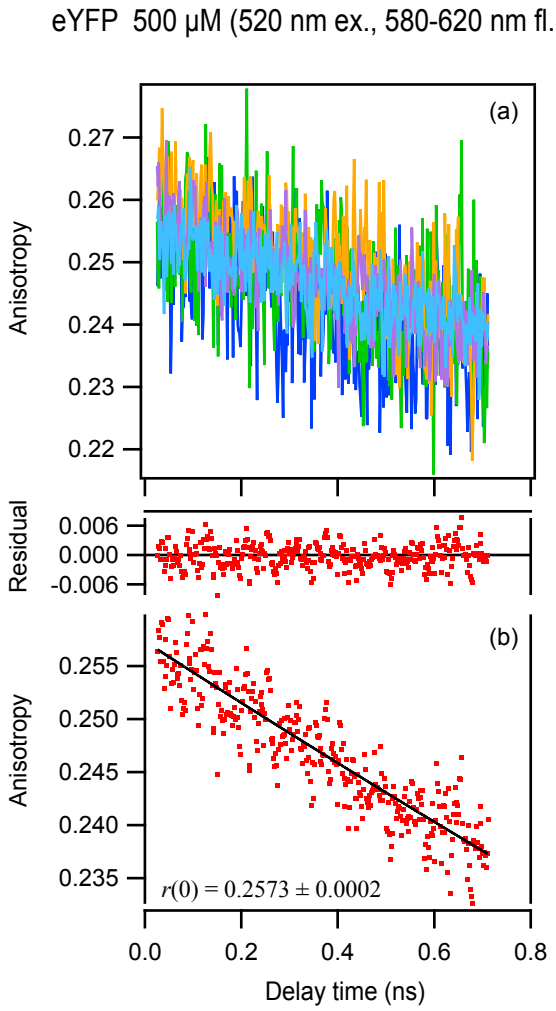

Figure S31. (a) Superposition of fluorescence anisotropy decay curves for 1-ns range measurements (5 accumulations) of 500 µM eYFP (PBS, pH 7.4). The corresponding average is shown in (b). The excitation wavelength was 520 nm, and fluorescence was collected over 540–620 nm. The *G*-factor was 0.992. The average curve was fitted using a single-exponential function (eq 7), and the fitting curve and residuals are also plotted in (b). The anisotropy value at time 0, $r(0)$, with the standard error is shown in (b).

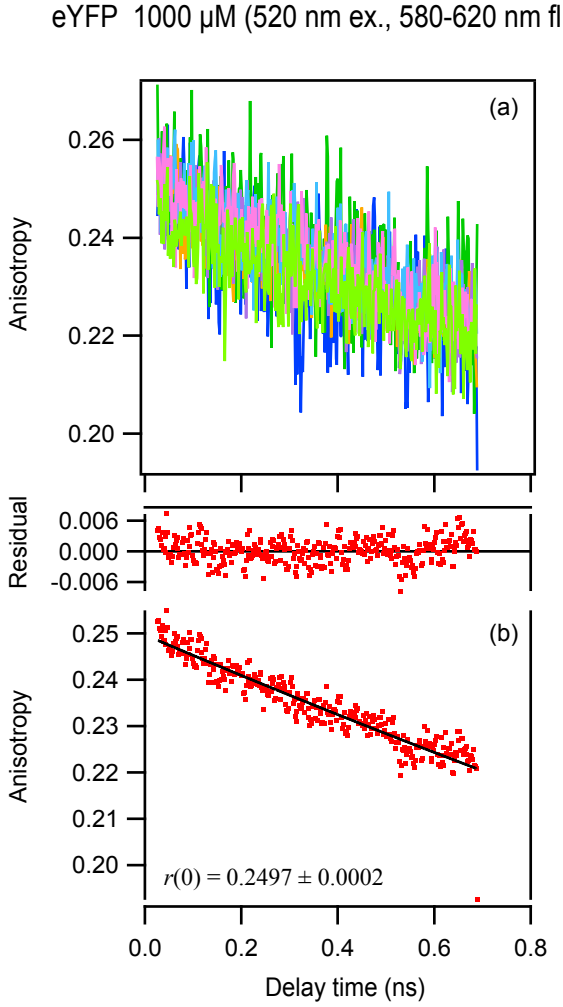

Figure S32. (a) Superposition of fluorescence anisotropy decay curves for 1-ns range measurements (7 accumulations) of 1000 μM eYFP (PBS, pH 7.4). The corresponding average is shown in (b). The excitation wavelength was 520 nm, and fluorescence was collected over 540–620 nm. The *G*-factor was 0.992. The average curve was fitted using a single-exponential function (eq 7), and the fitting curve and residuals are also plotted in (b). The anisotropy value at time 0, $r(0)$, with the standard error is shown in (b).

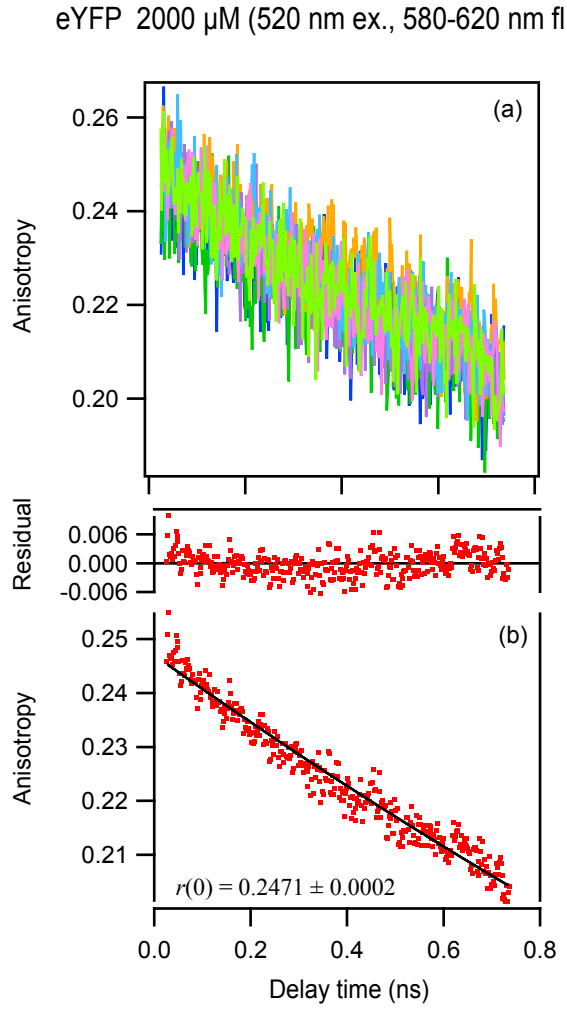

Figure S33. (a) Superposition of fluorescence anisotropy decay curves for 1-ns range measurements (7 accumulations) of 2000 µM eYFP (PBS, pH 7.4). The corresponding average is shown in (b). The excitation wavelength was 520 nm, and fluorescence was collected over 540–620 nm. The *G*-factor was 0.992. The average curve was fitted using a single-exponential function (eq 7), and the fitting curve and residuals are also plotted in (b). The anisotropy value at time 0, $r(0)$, with the standard error is shown in (b).

SI-7. Fluorescence anisotropy decay curves of eGFP A206K and eYFP A206K at high concentrations.

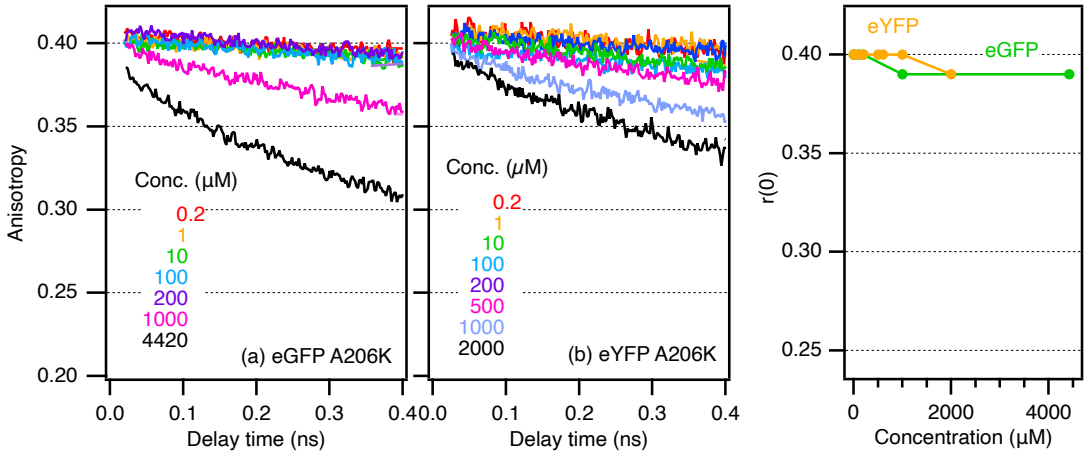

Figure S34. Fluorescence anisotropy decay curves of (a) eGFP A206K and (b) eYFP A206K, over a concentration range from 0.2 to 4420 μM (PBS, pH 7.4). (c) Concentration dependence of the anisotropy value at time 0, $r(0)$, for eGFP A206K and eYFP A206K. The excitation and emission wavelengths are the same as those described in Figure 6.

SI-8. Superimposition of the crystal structures of eGFP and YFP.

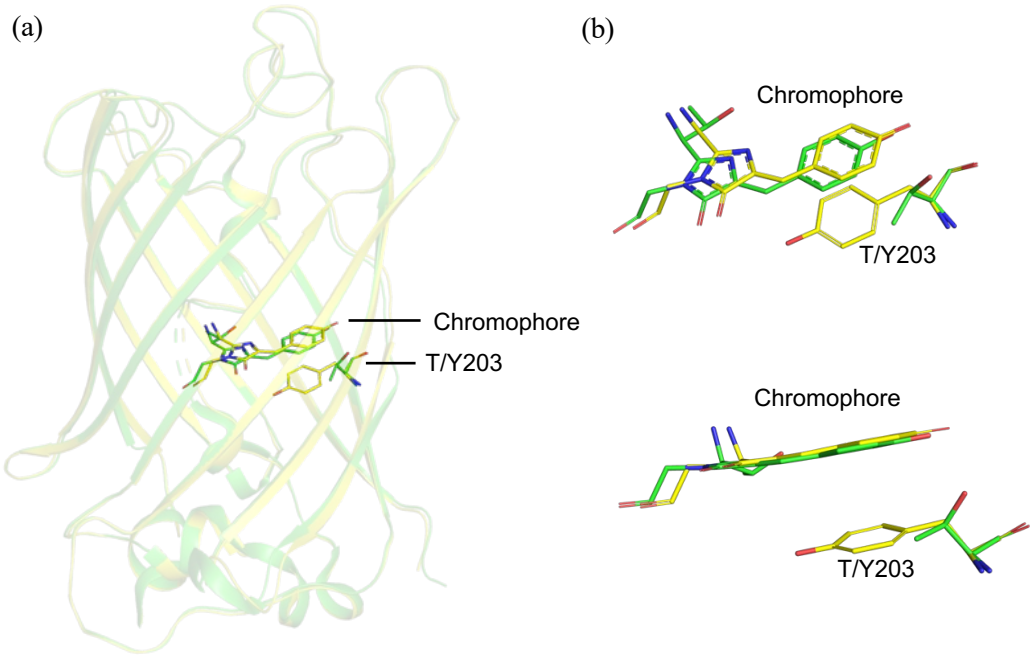

Figure S35. Superimposition of the structures aligned by α-carbon atoms of eGFP (PDB:2Y0G;[3] green) and YFP (PDB:1YFP;[4] yellow). (a) Overall structures. (b) Magnified view around the chromophore.

SI-9. Effect of 203rd Residue on Dimerization behavior of eYFP.

The Y203T mutation alters the absorption spectrum of eYFP. The anionic band exhibits a blue shift to 502 nm (Figure S36a), which results from the loss of the π–π stacking between the chromophore and Tyr203. Notably, this peak wavelength is not identical to that of eGFP (489 nm), which suggests that other residue differences between eGFP and eYFP also contribute to the electronic state of the chromophore. However, as shown in Figure S36b, the anisotropy decay curves for the eYFP Y203T mutant are nearly identical to those of eYFP at the same concentrations of both 10 μM and 200 μM.

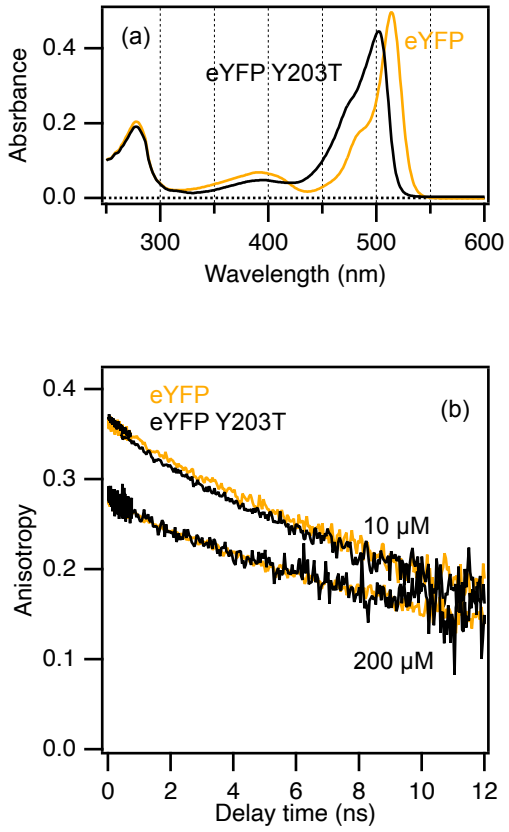

Figure S36. (a) Absorption spectra (10 μM) and (b) fluorescence anisotropy decay curves (10 μM and 200 μM) for eYFP and eYFP Y203T. The excitation wavelength was 520 nm. Fluorescence signals were collected over 540–620 nm. All measurements were performed in PBS.

SI-10. References.

1. D. K. McRorie and P. J. Voelker, Self-associating systems in the analytical ultracentrifuge, Beckman Instruments, Inc., Fullerton, CA, 1993.
2. T. M. Laue and W. F. S. III, *Annu. Rev. Biophys. Biomol. Struct.*, 1999, **28**, 75-100.
3. A. M. Kelley and D. F. Kelley, *J. Phys. Chem. Lett.*, 2022, **13**, 11942-11945.
4. A. D. Scully, A. Matsumoto and S. Hirayama, *Chem. Phys.*, 1991, **157**, 253-269.
5. Y. Sakai, M. Kawahigashi, T. Minami, T. Inoue and S. Hirayama, *J. Lumin.*, 1989, **42**, 317-324.
6. H. Tsubota, A. Takayama, Y. Takeda, N. Yamada and H. Hosoi, *J. Phys. Chem. B*, 2021, **125**, 7997-8009.